JCI The Journal of Clinical Investigation

Linear ubiquitin assembly complex regulates lung epithelial driven responses during influenza infection

Patricia L. Brazee, … , Laura A. Dada, Jacob I. Sznajder

J Clin Invest. 2019. https://doi.org/10.1172/JCI128368.

Research In-Press Preview Inflammation Pulmonology

Graphical abstract

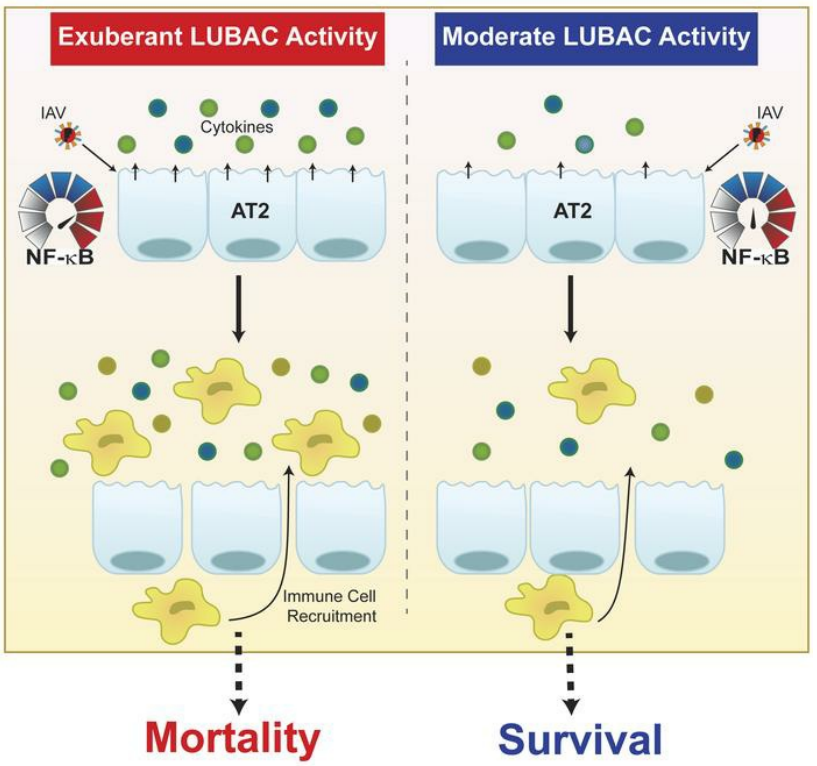

Linear ubiquitin assembly complex regulates lung epithelial driven responses during influenza infection

Patricia L. Brazee[1], Luisa Morales-Nebreda[1], Natalia. D. Magnani[1†], Joe G.N. Garcia[2], Alexander .V. Misharin[1], Karen M. Ridge[1], G.R. Scott. Budinger[1], Kazuhiro Iwai[3], Laura A. Dada[1*] and Jacob I. Sznajder[1*]

***** Denotes co-corresponding authors

Authors affiliations:

[1] Department of Medicine, Division of Pulmonary and Critical Care Medicine, Northwestern University, Chicago, IL, USA

[2] Department of Medicine, University of Arizona, Tucson, Arizona, USA

[3] Department of Molecular and Cellular Physiology, Graduate School of Medicine, Kyoto University, Yoshida-konoe-cho, Sakyo-ku, Kyoto, Japan

[†]Present address: Universidad de Buenos Aires. CONICET. Instituto de Bioquímica y Medicina Molecular (IBIMOL), Departamento de Química Analítica y Fisicoquímica. Cátedra de Química General e Inorgánica Facultad de Farmacia y Bioquímica. Buenos Aires, Argentina.

To whom the correspondence should be addressed:

Jacob I. Sznajder, Email: j-sznajder@northwestern.edu, Phone: 312-908-7737

Laura A. Dada, Email: lauradada@northwestern.edu, Phone: 312-503-5397

Division of Pulmonary and Critical Care Medicine

Northwestern University Feinberg School of Medicine

303 E Superior Street, Simpson Querrey 5-300

Chicago, IL 60611, USA.

Conflict of interest:

The authors have declared that no conflict of interest exists.

Abstract

Influenza A virus (IAV) is among the most common causes of pneumonia related death worldwide. Pulmonary epithelial cells are the primary target for viral infection and replication and respond by releasing inflammatory mediators that recruit immune cells to mount the host response. Severe lung injury and death during IAV infection results from an exuberant host inflammatory response. The linear ubiquitin assembly complex (LUBAC), composed of SHARPIN, HOIL-1L and HOIP, is a critical regulator of NF-κB-dependent inflammation. Using mice with lung epithelial specific deletions of HOIL-1L or HOIP in a model of IAV infection, we provided evidence that, while a reduction in the inflammatory response was beneficial, ablation of the LUBAC-dependent lung epithelial-driven response worsened lung injury and increased mortality. Moreover, we described a mechanism for the upregulation of HOIL-1L in infected and non-infected cells triggered by the activation of type I interferon receptor and mediated by IRF1, which was maladaptive and contributed to hyper-inflammation. Thus, we propose that lung epithelial LUBAC acts as a molecular rheostat that could be selectively targeted to modulate the immune response in patients with severe IAV-induced pneumonia.

Introduction

Seasonal influenza A viral infection affects a significant proportion of the population in the United States and worldwide. While most patients infected with influenza A virus (IAV) recover without major sequelae, severe viral pneumonia is one of the most common causes of acute respiratory distress syndrome (ARDS) (1-4) . Impairment of gas exchange in IAV-induced ARDS, in large part, is due to damage to the alveolar epithelial barrier and edema accumulation (1, 4-6). During IAV infection an exaggerated inflammatory response, known as “cytokine storm”, can occur which disrupts the alveolar epithelial barrier and leads to the development of ARDS (5), increasing IAV-induced morbidity and mortality.

Alveolar epithelial cells (AEC) are targets of IAV infection and orchestrate the host immune response necessary for viral clearance (7, 8). As IAV replicates within AEC, viral particles accumulate in the cytosol and are sensed by the host pattern recognition receptor retinoic acid-inducible gene I (RIG-I), inducing the production of cytokines and interferons (9-11). AEC-derived cytokines and interferons promote recruitment of host immune cells which release additional cytokines and proteases in an effort to limit viral spread (5). However, the non-specific nature of the innate immune response can damage non-infected adjacent cells (5, 7). As AEC die, either by direct infection or as a consequence of the inflammatory response, the alveolar barrier becomes permeable to solutes leading to edema accumulation and impaired gas exchange (5, 7, 12). Data from animal models of severe IAV infection suggest that “cytokine storm” is the major driver of morbidity and mortality (13-17). Several studies suggest that reductions in circulating cytokines improve lung injury and survival, highlighting the importance of modulating the host inflammatory response during IAV infection (14, 18, 19).

The linear ubiquitin assembly complex (LUBAC) is essential for NF-κB activation, where it targets the NF-κB essential modulator (NEMO) for linear ubiquitination (20-24). LUBAC is an E3-ligase complex composed of the accessory protein, Shank-Associated RH domain-Interacting Protein (SHARPIN), as well as two RING-in-between-RING ligases: the Heme-Oxidized Iron responsive element binding protein 2 ubiquitin Ligase-1L (HOIL-1L) and the catalytically active component HOIL-1-Interacting Protein (HOIP) (20, 25, 26). Unlike most ubiquitin E3 ligases, which utilize the internal lysine residues of ubiquitin, LUBAC forms Met-1-linked head-to-tail linear ubiquitin chains (20, 22, 25). While the exact stoichiometry of the 600 kDa complex has yet to be

elucidated, the presence of all three LUBAC components is necessary for its stability and maximal activity, despite HOIP being the only catalytically active component of the complex (25, 27). Predominantly studied downstream of TNF receptor superfamily (TNFRSF), linear ubiquitin chains on NEMO stabilize the IκB kinase (IKK) complex, consisting of NEMO, IKKα and IKKβ, enabling the phosphorylation and degradation IκBα, releasing NF-κB to translocate to the nucleus, stimulating downstream inflammation (21, 28, 29). NEMO can also form a complex that can activates interferon regulatory factor 3 (IRF3), initiating its dimerization and translocation to the nucleus, where it drives type I interferon production to modulate the antiviral response (30). While the role of LUBAC in NF-κB signaling downstream of TNFRSF has been well established, the role of alveolar epithelial LUBAC in regulating NF-κB-dependent inflammation downstream of RIG-I during IAV infection is unknown.

In this study, we report that the degree of LUBAC activity determines the alveolar epithelial-driven inflammatory response to IAV infection. During IAV infection, type I interferon upregulates HOIL-1L expression in AEC and thus enhances LUBAC formation, leading to an exaggerated inflammatory response and severe lung injury. In agreement with a role of alveolar epithelial LUBAC driving the lung inflammatory response, reducing the complex formation by using a transgenic mice with a lung epithelial cell-specific deletion of HOIL-1L protected mice from severe lung injury and increased survival. Moreover, complete loss of lung epithelial LUBAC activity, as observed in mice with a genetic deletion of HOIP from the lung epithelium, worsened outcomes during IAV infection. As such, this work uncovers a novel role for LUBAC as a rheostat of the epithelial-driven inflammatory response to IAV infection, which could be targeted as a potential therapeutic strategy for control of IAV-induced cytokine storm to improve patient outcomes during severe infection.

Results

Linear ubiquitin chains regulate the NF-κB response to IAV downstream of RIG-I signaling

We infected an alveolar epithelial cell line (A549) with H1N1 A/WSN/1933 (WSN) at 1 MOI, for 16 hours, a dose and time at which we observed RIG-I-dependent NF-κB and IRF3 activation (measured by the phosphorylation relative to total IκBα and IRF3 respectively), NEMO ubiquitination, and cytokine production (Figure 1, Supplemental Figure 1A-C). After siRNA silencing of either HOIL-1L or HOIP, we detected no appreciable differences in RIG-I activation as compared to control siRNA treated cells in response to WSN infection (Figure 1B-C, Supplemental Figure 1D-E). However, analysis of NEMO-ubiquitination after immunoprecipitation from cell lysates showed that loss of LUBAC components resulted in a graded decrease of linear chains, were silenced HOIL-1L reduced their abundance and siHOIP inhibited the linear ubiquitin of NEMO during IAV infection (Figure 1D). Downstream of NEMO linear ubiquitination, silencing of HOIL-1L or HOIP decreased in the IAV-induced activation of NF-κB and IRF3 as well as the secretion of IL-6 and IFN-β in a similarly graded manner (Figure 1E-G, Supplemental Figure 1F-G). Together these results suggest that LUBAC regulates the inflammatory and antiviral response downstream of RIG-I signaling in response to IAV.

Loss of HOIL-1L from the lung epithelium reduces lung injury and improves survival in mice infected with IAV

To evaluate whether LUBAC activity in the lung epithelium regulates IAV induced lung injury, we generated mice with a tissue specific deletion of full length HOIL-1L (SPC^{cre}/$HOIL\text{-}1L^{fl/fl}$) (31). These mice were generated using the same construct described for the well defined $HOIL\text{-}1L^{-/-}$ mice (21, 31), which do not express full length HOIL-1L, but instead express a 30kDa truncated variant (21) that results in reduced levels of 600 kDa LUBAC (32) as well as impaired NF-κB signaling (21). Immunoblots of mouse alveolar type 2 (AT2) cells lysates using either a specific antibody against the C- terminus (21, 31) or N-terminus of HOIL-1L (33), showed a band at approximately 55 kDa in WT AT2 cells, corresponding to the molecular weight of full-length HOIL-1L, that was absent in SPC^{cre}/$HOIL\text{-}1L^{fl/fl}$ AT2 cell lysates (Supplemental Figure 2A-b). Additionally, using the HOIL-1L N-terminus antisbody we observed a low abundance band at approximately 30 kDa in SPC^{cre}/$HOIL\text{-}1L^{fl/fl}$ AT2 cells (Supplemental Figure 2A) (33). This observation is in agreement with the description of the 30 kDa band in lysates from $HOIL\text{-}1L^{-/-}$ mice which represents a truncated splice variant of HOIL-1L lacking the C-

terminal RING domain but retaining its ubiquitin-like (UBL) domain for interaction with HOIP as well as its LUBAC-tethering motif (LTM) necessary for interactions with SHARPIN (21, 33, 34). The absence of HOIL-1L can destabilize the complex and decrease HOIP and SHARPIN expression (27, 33, 35), however, we observe no significant change in HOIP expression between WT and SPC^{cre}/HOIL-1L$^{fl/fl}$ AT2 cells (Supplemental Figure 2B). Interestingly, we observed a slight increase in SHARPIN expression in SPC^{cre}/HOIL-1L$^{fl/fl}$ AT2 cells compared to WT (Supplemental Figure 2B). SHARPIN is sufficient to stabilize HOIP and promote LUBAC activity in the absence of HOIL-1L , albeit with lower efficiency compared with complexes containing HOIL-1L (27), supporting the notion that respiratory epithelial cells in SPC^{cre}/HOIL-1L$^{fl/fl}$ mice retain some degree of LUBAC activity.

WT and SPC^{cre}/HOIL-1L$^{fl/fl}$ mice were infected intratracheally (i.t.) with a low or lethal dose of WSN and monitored for survival. Low dose WSN infection resulted in ~75% survival of SPC^{cre}/HOIL-1L$^{fl/fl}$ mice compared to 40% in WT mice at 20 days post infection (d.p.i.) (Figure 2A). A lethal dose of WSN, resulted in 100% mortality of WT mice by 12 d.p.i., while ~20% SPC^{cre}/HOIL-1L$^{fl/fl}$ mice survived. The differences in mortality during infection with WSN corresponded with decreased severity of lung injury in SPC^{cre}/HOIL-1L$^{fl/fl}$ mice, assessed by measuring total protein content in bronchoalveolar lavage fluid (BALF), which was decreased by ~25% at 5 d.p.i. and ~20% at 7 d.p.i. with the lethal dose as compared to WT mice (Figure 2B). In agreement with reduced barrier permeability, at the same time points we detected a significant decrease in total cell count in BALF in SPC^{cre}/HOIL-1L$^{fl/fl}$ mice as compared to WT mice (Figure 2C). Careful examination of multiple parameters in H&E stained lung sections, including peribronchial infiltration, bronchial exudate, alveolar infiltration, and thickening of alveolar walls showed reduced severity of lung injury in SPC^{cre}/HOIL-1L$^{fl/fl}$ mice as compared to WT at 7 d.p.i. with low dose WSN (Supplemental Figure 2C-D). Moreover, in WT mice we observed that a lethal dose of WSN resulted in peak viremia at 5 d.p.i. which was decreased by 27% in SPC^{cre}/HOIL-1L$^{fl/fl}$ mice with no significant differences in clearance at 7 d.p.i. (Figure 2D).

BALF samples from WT and SPC^{cre}/HOIL-1L$^{fl/fl}$ mice were further analyzed to determine cytokine content after lethal WSN infection. WT mice infected with WSN had high levels of IL-6 (Figure 3A), MCP-1, and IFN-γ by 5 d.p.i. that remained elevated through 7 d.p.i., all of which were significantly reduced in the BALF of WSN infected SPC^{cre}/HOIL-1L$^{fl/fl}$ mice (Supplemental Figure 2E-F), while BALF levels of TNF-α were similarly

elevated in both strains (Supplemental Figure 2G). Additionally, at 3 and 5 d.p.i. type I interferons (IFN-α, IFN-β) were significantly reduced in SPC^{cre}/HOIL-1L$^{fl/fl}$ compared to WT mice (Figure 3B-C). Conversely, at 7 d.p.i. BALF from SPC^{cre}/HOIL-1L$^{fl/fl}$ mice contained 2-fold higher levels of the anti-inflammatory cytokine IL-10 (Supplemental Figure 2H). At 5 d.p.i. we also observed reduced levels of IL-1β in the BALF of SPC^{cre}/HOIL-1L$^{fl/fl}$ mice compared to WT mice (Supplemental Figure 2I) that corresponded with reduced *Il1b* transcription in isolated SPC^{cre}/HOIL-1L$^{fl/fl}$ AT2 (Supplemental Figure 2J) with no defect in SPC^{cre}/HOIL-1L$^{fl/fl}$ AT2 inflammasome activation compared to WT AT2 at 5 d.p.i (Supplemental Figure 2K). Taken together these results suggest that loss of full length HOIL-1L from lung epithelial cells confers protection during IAV infection by altering the ratio of pro-inflammatory and anti-inflammatory cytokines and reducing the levels of interferons.

AEC-derived cytokines and interferons promote recruitment and activation of immune cells (5). To determine the effect of loss of HOIL-1L on the innate immune response, we analyzed lung myeloid and lymphoid populations in WT and SPC^{cre}/HOIL-1L$^{fl/fl}$ lungs at 0, 3, 5, and 7 d.p.i. by flow cytometry using defined lineage specific cell surface markers and gated as described in Methods and Supplemental Figure 3A-B (36). In WT mice, we observed a significant increase in the number of CD11b^{hi}MHCII^{low}Ly6C^{hi} classical monocytes after WSN infection which was blunted in SPC^{cre}/HOIL-1L$^{fl/fl}$ mice at all time points (Figure 3D). Similarly, recruitment of CD11b^{hi}MHCII^{hi}CD24^{low}CD64^{hi} monocyte-derived inflammatory macrophages was decreased by 45% in SPC^{cre}/HOIL-1L$^{fl/fl}$ mice as compared to WT mice at 7 d.p.i. (Figure 3E). While NK1.1^{+}CD11b^{int} NK cells were increased by 2-fold in the airspace of WT mice, NK cell numbers were significantly reduced in the lungs of SPC^{cre}/HOIL-1L$^{fl/fl}$ mice at the same time points (Figure 3F). Additionally, numbers of tissue resident SiglecF^{hi}CD11c^{hi} alveolar macrophages and Ly6G^{+}CD11b^{hi}CD24^{hi} neutrophils during IAV infection were similar in WT and SPC^{cre}/HOIL-1L$^{fl/fl}$ mice (Supplemental Figure 2G-H). While the innate response is important to limit viral spread, clearance of IAV from an infected host is dependent on the adaptive response (37, 38). Analysis of lung lymphoid populations by flow cytometry (Supplemental Figure 3B) after IAV infection showed a significant increase in the number of CD44^{+}CD62L^{-}CD8^{+} effector T cells and of CD4^{+}CD25^{+}Foxp3^{+} T_{reg} cells in infected SPC^{cre}/HOIL-1L$^{fl/fl}$ mice compared to WT mice (Figure 3G-H) In contrast, no differences were detected in the number of CD44^{+}CD62L^{-}CD4^{+} T cells between WT and SPC^{cre}/HOIL-1L$^{fl/fl}$ mice post infection

(Supplemental Figure 2I). Taken together these data suggest that LUBAC-dependent signaling at the epithelial level impacts multiple facets of the host immune response during IAV infection.

To determine the impact of the decrease in viral titers (Figure 2D) on the protection from lung injury and decreased inflammation in IAV-infected SPC^{cre}/HOIL-1L$^{fl/fl}$ mice, we administered a higher dose of WSN (WSN^{Higher}) which resulted in viral titers at peak viremia comparable to those in WT mice infected with the standard lethal dose of WSN (WSN^{StdL}) used in our in vivo model (Supplemental Figure 4A). SPC^{cre}/HOIL-1L$^{fl/fl}$ mice which received WSN^{Higher} continued to display significantly reduced alveolar permeability, cellular infiltration, and IL-6 levels in BALF as compared to WT mice which received WSN^{StdL} (Supplemental Figure 4B-D). We observed no significant differences in BALF IFN-β levels between WSN^{StdL} treated WT mice and WSN^{Higher} treated SPC^{cre}/HOIL-1L$^{fl/fl}$ mice (Supplemental Figure 4E). These data suggests that decreased viral load does not drive the ameliorated lung injury in SPC^{cre}/HOIL-1L$^{fl/fl}$ mice.

IAV infection increases HOIL-1L in alveolar epithelial cells

Analysis of the effect of IAV infection on the expression of LUBAC components revealed a significant upregulation of HOIL-1L at both the mRNA and protein levels by 3 d.p.i. through 7 d.p.i. (Figure 4A-B) in AT2 cells isolated from WT mice infected with WSN. No differences in HOIP or SHARPIN expression were detected (Supplemental Figure 5A-D). Similarly, when A549 cells were infected with 1 MOI WSN for 0, 4, 8, and 16 hours, we measured a 5-fold increase in *HOIL-1L* mRNA and a 2-fold increase in HOIL-1L protein abundance by 16 hours post infection (h.p.i.) (Supplemental Figure 5E-F), again, with no changes in expression of the other LUBAC components (Supplemental Figure 5G-J).

In addition to its role in stabilizing LUBAC to promote maximal activity of the complex (21, 27), it has been described that HOIL-1L has several LUBAC-independent functions, such as acting as an E3 ubiquitin ligase to target proteins such as PKCζ for degradation as seen in adaptation to hypoxia and cancer (23, 31, 39). Non-denaturing native gel electrophoresis of lysates from WT AT2 cells or A549 cells exposed to WSN in vitro revealed that HOIL-1L runs consistent with the migration of HOIP, to suggest association with LUBAC (25) (Figure 4C, Supplemental Figure 5K). These results suggest that during IAV infection newly synthesized HOIL-1L is incorporated into LUBAC.

IAV infection upregulates HOIL-1L via autocrine and paracrine type I interferon signaling

It has been described that virus infected epithelial cells signal to adjacent non-infected cells through the release of mediators, such as lipids, cytokines, and interferons (12, 40, 41). We sought to investigate whether the increase in HOIL-1L expression was a direct consequence of viral infection, a response to secreted autocrine and paracrine mediators, or both. At 0 and 3 d.p.i., single cell whole lung suspensions of WT AT2 cells, defined as $CD45^-$ $CD31^-$ $EpCam^+$, were FACS sorted based on the presence of the viral surface protein HA to separate infected (HA^+) from non-infected (HA^-) AT2 cell populations (Supplemental Figure 3C). Infection status of each population was confirmed by qRT-PCR, expression of IAV nucleoprotein (*NP*) (a viral genome associated protein necessary for replication in target cells) (Supplemental Figure 5L) (42). Analysis of mRNA from HA^- and HA^+ populations showed that infection with IAV was not required for HOIL-1L upregulation, as *HOIL-1L* mRNA was equally upregulated in both HA^- and HA^+ populations (Figure 4D). These results were recapitulated in vitro, where UV-irradiated conditioned media from untreated (CM^-) or IAV infected (CM^+) A549 cells was added to naïve cells. In response to CM^+, a 2-fold induction of HOIL-1L was detected as early as 12 h.p.i., which was inhibited by heat denaturation of protein mediators within CM^+ (Figure 4E). Taken together these results suggest that a protein mediator released from IAV-infected epithelial cells is sufficient to upregulate HOIL-1L in an autocrine or paracrine manner.

We next sought to identify the cytokine(s) necessary for the observed autocrine/paracrine regulation of HOIL-1L. It has been reported that IFN-α and IFN-γ can regulate the expression of LUBAC components in SHARPIN deficient mice (43). In our model, increased type I interferon (IFN-α, IFN-β) production in vivo paralleled HOIL-1L upregulation (Fig 3B-C). Thus, we tested whether IFN-α was sufficient to increase HOIL-1L expression by treating A549 cells with recombinant human IFN-α, and found a significant increased HOIL-1L expression in A549 cell lysates (Figure 4F). Additionally, AT2 cells isolated from type 1 interferon receptor (IFNAR1) deficient mice ($IFNAR1^{-/-}$) exposed to CM^+ failed to upregulate HOIL-1L as compared to WT AT2 cells (Figure 4G). We obtained similar results with in vitro siRNA silencing of IFNAR1 compared to siControl transfected A549 cells treated with CM^+ (Supplemental Figure 5M). To investigate whether direct viral infection was sufficient to induce HOIL-1L expression independent of IFNAR1 signaling, AT2 cells from $IFNAR1^{-/-}$ mice were infected with WSN. IFNAR1 deficiency inhibited HOIL-1L upregulation as compared to WSN infected WT AT2 cells,

despite active virus replication as measured by expression of the IAV non-structural protein 1 (NS1) (Supplemental Figure 5N). In vitro silencing of IFNAR1 yielded similar results, with inhibition of HOIL-1L upregulation as compared to siControl A549 cells treated with WSN (Supplemental Figure 3N). Conversely, upon CM^+ (Supplemental Figure 5O) or WSN treatment (Fig, 5I), AT2 cells isolated from mice lacking the receptor for CCL-2/MCP1 (CCR2) upregulated HOIL-1L expression comparable with WT AT2 cells. These results suggest that signaling downstream of IFNAR1 is necessary to induce HOIL-1L expression in both human and mouse AEC.

We sought to identify the transcription factor(s) regulating HOIL-1L downstream of IFNAR1. Interferon regulatory factors (IRF1-9) bind to variations of the interferon stimulated response element consensus sequence (44, 45) found within the HOIL-1L promoter (43). In silico analysis (46) of the human and mouse HOIL-1L promoters identified a shared putative binding site for IRF1. To validate a direct role of IRF1 in HOIL-1L regulation we performed a ChIP assay, revealing a 5-fold increase in the direct binding of IRF1 to the HOIL-1L promoter during WSN infection of A549 cells (Figure 4J). Additionally, in vitro silencing of IRF1 inhibited HOIL-1L upregulation in response to CM^+ (Figure 4K). Collectively, the data suggest that IRF1 binds to HOIL-1L promoter and regulates HOIL-1L induction in response to influenza-induced type I interferon signaling.

Deletion of epithelial HOIP during IAV infection worsens lung injury and decreases survival

To further assess the role of LUBAC in regulating the epithelial driven immune response to IAV, we generated a transgenic mouse with HOIP excised specifically from the lung epithelium ($SPC^{cre}/HOIP^{fl/fl}$) as described in Methods. Loss of HOIP protein levels, as well as the presence of HOIL-1L and SHARPIN was confirmed by immunoblot of WT and $SPC^{cre}/HOIP^{fl/fl}$ AT2 cell lysates (Supplemental Figure 6A). Administration of low dose WSN to $SPC^{cre}/HOIP^{fl/fl}$ mice significantly decreased survival compared to WT mice with a mean survival of 11.5 and 13 d.p.i. respectively (Figure 5A). Additionally, careful examination of multiple parameters in H&E stained lung sections showed enhanced severity of lung injury in $SPC^{cre}/HOIP^{fl/fl}$ mice as compared to WT at 7 d.p.i. (Supplemental Figure 6B-C). The lethal dose of WSN resulted in 100% mortality in both WT and $SPC^{cre}/HOIP^{fl/fl}$ mice by day 10 d.p.i., however, at earlier time points we observed differences in markers of lung injury, i.e. increased BALF protein (Figure 5B), and cell count (Figure 5C). Analysis of whole lung by plaque assay revealed an increase in viral load in $SPC^{cre}/HOIP^{fl/fl}$ mice as compared to WT mice at peak

viremia 5 d.p.i. with no significant differences in viral clearance by 7 d.p.i. (Figure 5D). Consistent with our observations that loss of alveolar epithelial HOIP expression is detrimental in the response to IAV infection, data mined from a previously reported genome wide association study data set of 232 African American patients with ARDS and 162 at-risk control subjects (47) revealed a SNP in HOIP gene (rnf31) which coincides with worsened ARDS prognosis (Supplemental Figure 7). The identified SNP results in an amino acid change from valine to isoleucine (V1061I) between the RING2 and LDD domains of HOIP that make up the "catalytic core" (22, 27). Together these results support our findings in SPC^{cre}/HOIL-1L$^{fl/fl}$ mice that a degree of LUBAC activity is protective during inflammatory lung injury, as inhibition of LUBAC in SPC^{cre}/HOIP$^{fl/fl}$ mice results in greater morbidity and mortality.

AT2 cells isolated from SPC^{cre}/HOIP$^{fl/fl}$ mice at 0 and 4 d.p.i. have a markedly impaired NF-κB response as shown by significantly decreased mRNA encoding *Mcp1*, *Il6*, and *Ifnb* compared to AT2 cells isolated from WT mice (Figure 6A-C). However, analysis of BALF revealed similar levels of IL-6 and MCP-1 between WT and SPC^{cre}/HOIP$^{fl/fl}$ mice over the course of infection (Figure 6D-E) while IFN-β levels were dampened in SPC^{cre}/HOIP$^{fl/fl}$ mice compared to WT mice at 5 d.p.i. (Figure 6F). Analysis of lung myeloid and lymphoid populations by flow cytometry at 0, 5, and 7 d.p.i. revealed similar recruitment of immune cell populations, in WT and SPC^{cre}/HOIP$^{fl/fl}$ mice (Figure 6G-H, Supplemental Figure 6D-F). We detected similar numbers of SiglecF^{hi}CD11c^{hi} alveolar macrophages (Supplemental Figure 6D), CD11b^{hi}MHCII^{hi}CD24^{low}CD64^{hi} monocyte-derived inflammatory macrophages (Supplemental Figure 6E), and CD11b^{hi}MHCII^{low}Ly6C^{hi} classical monocytes (Supplemental Figure 6F) in WT and SPC^{cre}/HOIP$^{fl/fl}$ mice. In contrast, we observed a significant reduction in neutrophil recruitment in SPC^{cre}/HOIP$^{fl/fl}$ mice as compared to WT mice at 5 d.p.i. (Figure 6G) as well as a 2-fold increase in the recruitment of NK1.1^{+}CD11b^{int} NK cells in SPC^{cre}/HOIP$^{fl/fl}$ mice as compared to WT mice at 7 d.p.i. (Figure 6H). Within the lymphoid lineage we detected a significant reduction in the number of CD44^{+}CD62L^{-}CD8^{+} T cells at 7.d.p.i. (Figure 6I) with no appreciable differences in the total number of either CD4^{+}CD25^{+}Foxp3^{+} T_{reg} cells or CD44^{+}CD62L^{-}CD4^{+} T cells in SPC^{cre}/HOIP$^{fl/fl}$ mice compared to WT mice (Supplemental Figure 6G-H). Together these results suggest that a certain amount of LUBAC activity at level of the lung epithelium is necessary to coordinate the proper host response to IAV infection and confer protection from lung injury.

Restoration of NF-κB signaling in SPC^{cre}/HOIP$^{fl/fl}$ mice reduces lung injury and improves survival during IAV infection.

LUBAC is necessary for robust NF-κB activation, as linear ubiquitin chains on NEMO provide a stable docking site for additional IKK complexes, facilitating efficient activation of IKKα and IKKβ, and phosphorylation and degradation of IκBα (21, 28, 29). To confirm that loss of LUBAC-dependent NF-κB signaling in AT2 cells was driving mortality in IAV infected SPC^{cre}/HOIP$^{fl/fl}$ mice, we utilized an adenovirus coding for the constitutively active form of IKKβ (AdIKKβ-CA) (48), the primary kinase responsible for phosphorylation of IκBα (49). SPC^{cre}/HOIP$^{fl/fl}$ mice were instilled a non-coding adenovirus (AdNull) or AdIKKβ-CA, 14 days before infection with WSN (Supplemental Figure 8A). Expression of IKKβ was confirmed by immunoblot of isolated AT2 cell lysates (Figure 7B). While no difference in the content of IL-6 or IFN-β levels in BALF was observed between naïve and AdNull treated SPC^{cre}/HOIP$^{fl/fl}$ mice was detected, IKKβ-CA was sufficient to induce their production (Supplemental Figure 8B-C). Taken together, these results suggest that overexpression of IKKβ-CA in SPC^{cre}/HOIP$^{fl/fl}$ mice is sufficient to restore epithelial driven NF-κB signaling downstream of LUBAC.

We next sought to determine if restoration of NF-κB signaling downstream of LUBAC in SPC^{cre}/HOIP$^{fl/fl}$ mice would impact survival during IAV infection. Low dose WSN infection resulted in 100% mortality by 15 d.p.i. in SPC^{cre}/HOIP$^{fl/fl}$ mice which received AdNull pre-treatment with AdIKKβ-CA resulted in significant protection (Figure 7A). Consistent with improved survival, we observed significant reductions in protein levels, infiltrating cell counts, and IL-6 in the BALF of SPC^{cre}/HOIP$^{fl/fl}$ mice administered AdIKKβ-CA as compared to AdNull treatment prior to WSN infection (Figure 7C-E). Experiments were performed 7 days post WSN infection, a time at which both AdNull and AdIKKβ-CA treated SPC^{cre}/HOIP$^{fl/fl}$ mice had lost a significant percentage of body weight (data not shown), but before any mortality events occurred (Figure 7A). Collectively, the data suggest that LUBAC-mediated NF-κB activation in lung epithelial cells is necessary for orchestration of a sufficient host response during IAV infection.

Discussion

IAV infection can cause severe pneumonia, respiratory failure and death (2, 4). A heterogeneous response to IAV with the same virulence exists within the population, suggesting that host factors play a crucial role regulating the inflammatory response and determining the severity of lung injury (2-4). While current anti-

influenza strategies are limited to yearly vaccination or administration of antiviral drugs, it is clear that inclusion of strategies that target the host pathways will be beneficial (7, 50). Here we report that the level of LUBAC activity in pulmonary epithelial cells is a critical determinant of the NF-κB inflammatory response to IAV infection. Tight regulation of NF-κB is critical for the maintenance of immune homeostasis as its uncontrolled activation may result in “cytokine storm” with severe pathological consequences (13-17). During IAV infection, expression of the LUBAC component HOIL-1L is upregulated in alveolar epithelial cells by a mechanism that involves direct binding of IRF1 to the HOIL-1L promoter in response to type I interferons (Figure 8). This upregulation of HOIL-1L during IAV infection appears to be maladaptive, as attenuation of LUBAC activity by silencing of full length HOIL-1L in the lung epithelium is protective. In contrast, we show that complete loss of LUBAC activity, via deletion of HOIP in lung epithelial cells, leads to impaired epithelial driven immune response and increased mortality. In support of these observations, a SNP predicted to result in an amino acid change in the “catalytic core” of HOIP was associated with a worse prognosis in a cohort of African American patients with ARDS compared with controls. These findings highlight the fine line between an excessive and an inadequate immune response and suggest that therapeutic modulation of LUBAC activity may be crucial, as it functions as a rheostat regulating the amplitude of the host response to IAV infection.

While several studies have focused on LUBAC signaling downstream of TNFRSF and the IL-1β receptor, changes in the expression of LUBAC components in these signaling pathways have not been reported (20-26, 34, 35, 51). In contrast, we observed that during IAV infection, HOIL-1L expression is increased and associates with the other LUBAC components. We found that the binding of IRF1 directly to the HOIL-1L promoter downstream of IFNAR1 is necessary for HOIL-1L upregulation during IAV infection in both human and mouse AEC. While we found type I interferon signaling to be necessary, we cannot discount the possible combinatorial role of additional factors, as IRF1 has also been shown to be upregulated in response to IFN-γ and TNF-α stimulation (43, 52, 53). We detected very low levels of TNF-α in BALF in response to IAV infection to suggest a minor, if any, role for TNF-α signaling in in vivo HOIL-1L upregulation. IFN-γ plays an important role in the antiviral response and has a robust effect on IRF1 induction (43, 53), and while we do not observe an increase IFN-γ until 5 d.p.i., it may contribute to maintaining elevated levels of HOIL-1L during IAV infection. The molecular mechanism responsible for the increased levels of HOIL-1L during IAV infection may be of great

interest as it may contribute to increased LUBAC stability and the exaggerated production of cytokines during IAV infection.

Expression of type I IFN early during infection restricts viral spread, both in the infected cell where interferon stimulated gene products directly target hijacked viral pathways, and in uninfected cells by priming an anti-viral state (17, 54). Due to the range of pathogenicity among IAV strains, divergent reports exist for the role of type I IFN signaling in limiting mortality during IAV infection (11, 55). However, a direct correlation between IAV-induced high IFN-α/β levels and high morbidity and mortality has been reported (11, 54, 56, 57). As the infection persists, an exuberant and sustained interferon response can have deleterious effects by enhancing TRAIL mediated cell death (11) or facilitating secondary bacterial infections (57). Thus, we propose that the interferon-mediated regulation of HOIL-1L as host maladaptation to IAV infection, as we observe significant protection in SPC^{cre}/$HOIL\text{-}1L^{fl/fl}$ mice. While HOIL-1L does not directly contribute to linear ubiquitin chain formation (23, 27) its binding within LUBAC masks an ubiquitination site on HOIP to prevent its proteasomal degradation and releases HOIP's auto-inhibitory fold to maximize LUBAC activity (23, 26, 27, 32). Thus, increased abundance of HOIL-1L may contribute to the enhanced stability and activity of LUBAC. As the stoichiometry of LUBAC has not been elucidated (23, 26, 27), increased LUBAC-associated HOIL-1L may represent an increase in the ratio of HOIL-1L within the complex or an increase in the abundance of LUBAC complexes, either of which contribute to enhanced NEMO linear ubiquitination and robust downstream NF-κB activation (Figure 8).

Loss of LUBAC activity has been shown to have cell type specific effects (23, 58-60). For example, patients with LUBAC deficiency present with both auto inflammation and immunodeficiency. In mice, global HOIP and HOIL-1L null mice are embryonically lethal, while global SHARPIN deficiency results in viability with multiorgan inflammation. In contrast, $HOIL\text{-}1L^{-/-}$ mice, which express a low level of truncated N-terminal HOIL-1L, which retains the UBL and LTM domains for heterotrimeric LUBAC formation (N-HOIL-1L) (33), are viable with no overt phenotype. To circumvent confounding cell type specific phenotypes in vivo, we utilized a pulmonary epithelial cell specific transgenic mouse model (SPC^{cre}). SPC^{cre}/$HOIL\text{-}1L^{fl/fl}$ mice lack full length HOIL-1L and express a low level N-HOIL-1L, and thus are capable of a certain level of LUBAC-dependent signaling. While it has been reported that influenza infection of mice with chronic proliferative dermatitis due to global SHARPIN

deficiency results in decreased survival compared to WT mice (61), here we have shown that IAV infection of phenotypically normal SPC^{Cre}/HOIL-1L$^{fl/fl}$ mice resulted in increased survival compared to WT mice. While the mice utilized in this study have low expression of the truncated variant of HOIL-1L and may retain some LUBAC activity, SPC^{cre}/HOIL-1L$^{fl/fl}$ mice have significantly reduced cytokine and interferon levels in response to IAV infection. This is consistent with our in vitro data were silencing of full length HOIL-1L reduced the linear ubiquitination of NEMO, activation of NF-κB and IRF3, and IL-6 and IFN-β secretion. Additionally, studies in which mouse embryonic fibroblasts derived from HOIL-1L$^{-/-}$ mice, which do not express full length HOIL-1L, but instead express the truncated variant (21) have reduced levels of 600 kDa LUBAC (32) as well as impaired NF-κB signaling (21). These findings suggest that deletion of full length HOIL-1L and low expression of the truncated N-terminal fragment, is sufficient to destabilize LUBAC, and reduce LUBAC-dependent inflammatory signaling. We find that fine-tuning of LUBAC activity, though deletion of lung epithelial full length HOIL-1L is protective during IAV infection, reducing lung injury, viral titers and promoting survival.

The effects of lung epithelial HOIL-1L deletion on the innate and adaptive immune responses to IAV infection suggest that multiple mechanisms may be responsible for the lower viral titers, reduced injury and improved survival in SPC^{cre}/HOIL-1L$^{fl/fl}$ mice compared with WT mice. During IAV infection respiratory epithelial cells produce large amounts of MCP-1, resulting in the recruitment of classical monocytes and inflammatory monocyte-derived macrophages which produce large amounts of cytokines and are the predominant cause of immune pathology during influenza infection (14, 56). NK cells recruited to the lung also contribute to tissue damage as they target infected AEC for destruction, sacrificing barrier integrity in an effort to limit viral spread (62, 63). As such, reductions in inflammatory cytokines, classical monocytes inflammatory monocyte-derived macrophages, and NK cells seen in IAV-infected SPC^{cre}/HOIL-1L$^{fl/fl}$ mice likely play a significant role in the protection from lung injury and increased survival during IAV infection. In addition, CD8^{+} T cells were increased in SPC^{cre}/HOIL-1L$^{fl/fl}$ mice as compared to WT mice. The specific targeting of infected AEC by CD8^{+} T cells, is the primary mode of viral clearance in the IAV-infected lung (64). While we show that the improved survival was not exclusively attributable to lower viral loads, as SPC^{cre}/HOIL-1L$^{fl/fl}$ mice remain protected after infection with a higher titer of virus, increased antiviral CD8^{+} T cells in SPC^{cre}/HOIL-1L$^{fl/fl}$ mice may contribute to the measured decrease in peak viral titers and contribute to potential long term survival. In support of this, it has

been reported that IAV infection of T cell deficient mice resulted in a lower survival rate by 21 d.p.i, persistent lung injury and higher viral titers compared to WT mice (64, 65). Moreover, there was a significant increase in the number of T_{reg} cells in SPC^{cre}/HOIL-$1L^{fl/fl}$ mice as compared to WT mice. T_{reg} cells contribute to both quelling the inflammatory response to limit tissue damage as well as the promotion of tissue repair (66). Together with the concurrent increased levels of the anti-inflammatory cytokine IL-10 in SPC^{cre}/HOIL-$1L^{fl/fl}$ mice as compared to WT mice, our results suggest reduced inflammation confers protection during IAV infection. This supported by clinical findings in patients with worse outcomes of the pandemic 2009 H1N1 IAV who had elevated levels of circulating IL-6 despite viral clearance (15). These findings highlight the ability of LUBAC-dependent lung epithelial signaling to coordinate multiple components of the immune responses to IAV infection.

A balance between an excessive and inadequate immune response to infection is necessary for optimal recovery from IAV infection. In contrast to SPC^{cre}/HOIL-$1L^{fl/fl}$ mice, genetic deletion of HOIP in lung epithelial cells resulted in worse lung injury and decreased survival in response to IAV infection. These findings are in agreement with worse ARDS prognosis associated with a SNP within the “catalytic core” of HOIP, which may affect its activity or protein-protein interactions necessary for NF-κB activation. AT2 cells from SPC^{cre}/$HOIP^{fl/fl}$ mice infected with a lethal dose of WSN had significantly reduced mRNA expression of inflammatory cytokines, while total BALF cytokine concentrations were comparable. As such, we believe another cell type is driving the inflammatory response to IAV infection in SPC^{cre}/$HOIP^{fl/fl}$ mice. It has been shown by several groups, in several models, (TNF-α, TRAIL, cisplantin) that loss of HOIP from a cell, sensitizes it to induction of cell death (51, 61, 67, 68). This enhanced cell death in the absence of HOIP may account for the alternative activation of inflammation, as dying cells can release damage-associated molecular patterns that can induce inflammation (69). LUBAC inhibits several proteins involved in the induction of both apoptosis and necroptosis, as well as stabilization of anti-apoptotic proteins, and expression of NF-kB dependent pro-survival genes. As such, loss of HOIP from the respiratory epithelium may have pleiotropic effects. Influenza virus can induce intrinsic cell death pathways to cause epithelial cell death, which would release damps that activate resident immune cells. As the epithelial barrier is damaged, inflammatory infiltrates can more easily fill the airspace and contribute to immunopathology.

Use of a constitutively active mutant of IKKβ to bypass linear ubiquitin-dependent signaling and restore the NF-κB pathway in HOIP-deficient cells improved survival and reduced lung injury in $SPC^{cre}/HOIP^{fl/fl}$ mice during IAV infection, further supporting the crucial role of LUBAC-dependent signaling in regulating the host response to IAV infection. $SPC^{cre}/HOIP^{fl/fl}$ mice reconstituted with constitutively active IKKβ have restored NF-κB signaling, including the production of IL-6 and IFN-β (Supplemental Figure 8B-C). As such, upon IAV infection, IKKβ-CA expressing $SPC^{cre}/HOIP^{fl/fl}$ alveolar epithelial cells are able to initiate host response by activating NF-κB downstream of LUBAC. In addition to the restored epithelial cells driven production of cytokines and interferons, rescue of the NF-κB pathway may induce the upregulation of pro-survival genes to reduce IAV-induced cell death pathways and contribute to the improved survival in AdIKKβ-CA treated $SPC^{cre}/HOIP^{fl/fl}$ mice. Collectively, restoration of the NF-κB pathway in $SPC^{cre}/HOIP^{fl/fl}$ respiratory epithelial cells shifts origination of the inflammatory to IAV response back to the epithelium. Taken together, our data underscore the critical importance of LUBAC mediated NF-κB signaling in the alveolar epithelium orchestration of the host response to viral infections.

In conclusion, we show that during IAV infection, the amplitude of the inflammatory response is modulated by alveolar epithelial LUBAC activity which serves as a molecular rheostat and regulates the host response. While several chemical inhibitors as well as peptides that bind HOIP have been used to inhibit LUBAC activity in cell culture (70-73) and in vitro assays (74, 75) and support the targetablility of LUBAC, we have demonstrated that complete loss of HOIP is detrimental during IAV infection, however, some destabilization of LUBAC through loss of HOIL-1L is beneficial. Thus, novel compounds which target LUBAC stability to modulate LUBAC activity may be therapeutically beneficial for the treatment of hyperinflammatory response during IAV infection, were a modest degree of host response is necessary.

Methods

Mouse strains

Mice were bred in a barrier facility at Northwestern University. $SPC^{cre}/Rbck1(HOIL\text{-}1L)^{fl/fl}$ mice on a C57BL/6 background were generated as previously described (31). $Rnf31(HOIP)^{fl/fl}$ mice were generated on a C57BL/6 background by Ozgene Pty Ltd. (Perth, Australia). Briefly, a conditional allele of HOIP was generated by flanking exon 6 with loxP sites, generating a translational frameshift and rendering downstream exons non-

functional. A neomycin cassette flanked by FRT sites was used for selection in embryonic stem cells. Subsequent breeding of wt/flox to wt/flp mice removed the neomycin cassette. Heterozygous crossing bred out *flp* and generated homozygous $HOIP^{fl/fl}$ mice. $HOIP^{fl/fl}$ mice were then bred to SPC^{cre} mice for the specific deletion of HOIP from alveolar epithelial cells. The $SPC^{cre}/HOIP^{fl/fl}$ colony was maintained by crossing $HOIP^{fl/fl}$ to $SPC^{cre}/HOIP^{fl/fl}$. Deletion was confirmed through genotyping (Transnetyx) and by immunoblotblot of AT2 lysates with specific antibodies. B6.129S2-$Ifnar1^{tm1Agt}$/Mmjax ($IFNAR1^{-/-}$) and B6.129S4-$Ccr2^{tm1Ifc}$/J ($CCR2^{-/-}$) mice were purchased from Jackson Laboratory and have been previously described (76) (85(77). Mice were provided with food and water ad libitum and maintained on a 14-h light/10-h dark cycle.

Histology

Lungs were fixed and processed as previously described (31). Brightfield images were obtained using TissueFAXS software (TissueGnostics). Quantification of severity of lung injury from H&E images was based peribronchial infiltration, bronchial exudate, and alveolar infiltration.

Reagents

The following pooled siRNA were purchased from Santa Cruz Biotechnology (Scbt) and used at the indicated concentrations: siRBCK1(HOIL-1L) (sc-61446, 60 pmol), siIRF1 (sc-35706, 70 pmol), siSHARPIN (sc-77833, 120 pmol), siIFNAR1 (sc-35637, 70 pmol), and a scrambled non-targeting control (sc-37007) at corresponding concentrations. Additional reagents include siHOIP(RNF31) (Qiagen #141713365, 120 pmol), Lipofectamine RNAiMAX (Fisher Scientific, #13778075), and recombinant human IFN-α (BioLegend, #592704, 100 U/mL).

Cell culture

A549 (ATCC), MDCK (ATCC) and AT2 cells isolated and cultured as previously described (31). Cell lines were routinely tested for mycoplasma contamination using the MycoAlert kit (Lonza).

Immunoprecipitation and Immunoblot analysis

Immunoprecipitation was performed as previously described (78). Briefly, protein concentrations were incubated with A/G agarose beads (Scbt, sc-2003) and an anti-NEMO antibody (1ug, Scbt, sc-8330) rotating overnight. Beads were washed 3 times in 1% w/v Triton X-100, 20 mM Tris–HCl (pH 7.5), 150 mM NaCl and eluted proteins analyzed by immunoblot. Immunoblotting was performed by resolving protein lysates on SDS-

PAGE gels (7.5-10 %), followed by transfer to nitrocellulose membranes (Bio-Rad) and further incubation of membranes with indicated antibodies overnight (see Supplemental Table 1). HRP-tagged secondary antibodies (Bio-Rad, 1721011 and 1721019) were used in combination with Super-Signal ECL kit (Thermo Fisher) to develop immunoblots using a LI-COR Odyssey Imager and companion software Image Studio version 5.2. Immunoblots were quantified using densitometry (ImageJ 1.46r; National Institutes of Health, Bethesda, MD) (19)**.**

Influenza A virus infection

Influenza A virus strain A/WSN/33(H1N1) was used for in vitro and in vivo experiments. A549 cells were seeded in 35 mm dishes at a density of $2x10^5$ cells per well and infected at 1 MOI for 16 hours in DMEM. Primary mouse AT2 cells were seeded in a 12 well plate format at a density of $3x10^6$ cells per well and infected at 1 MOI for 16 hours in DMEM. Conditioned media was removed from infected cells and exposed to UV light for 15 minutes on ice for virus inactivation before addition to naïve cells (79). As a control, UV-treated supernatant was boiled (99º C) for 10 minutes to denature proteins.

For in vivo infections, anesthetized mice were i.t. inoculated with WSN diluted in 50 μL sterile PBS as described (80). A dose of 500 plaque forming units (PFU) per mouse was used for lethal infections and 100 PFU for the sublethal dose. For survival studies, upon developing a moribund condition (slowed respiration, hunched posture, lack of curiosity, little or no response to stimuli and not moving when touched) mice were euthanized and recorded as IAV-induced mortality. BALF was collected using 1 mL of PBS instilled into the lungs and aspirated three times (81, 82).

Determination of viral titer

Whole lung homogenates were serially diluted in DMEM containing 1% BSA were added to MDCK cells followed by a standard plaque assay protocol (83). Plaques were counted at each dilution to calculate viral titer.

Flow cytometry and cell sorting

Multicolor flow cytometry and cell sorting were performed with an LSR Fortessa or BD FACSAria cell sorter using DIVA software (BD Biosciences). Analysis was performed off line using FlowJo software (v10.1).

Myeloid and lymphocyte populations from whole lung were isolated and defined as previously described (36, 84, 85). Briefly, perfused lungs were inflated with digestion buffer (1 mg/mL of Collagenase D and 0.1 mg/mL DNase I, both from Roche) and coarsely minced before processing in C-tubes (Miltenyi Biotec) with a GentleMACS dissociator (Miltenyi Biotec), according to the manufacturer's instructions. Homogenate was passed through 40-μm nylon mesh to obtain a single-cell suspension and subjected to red blood cell lysis (BD Pharm Lyse, BD Biosciences). Live cells were counted using a Countess cell counter (Invitrogen) by trypan blue exclusion.

Cells were stained with antibodies listed in Supplemental Table 2-3 and gated as described elsewhere (19, 36) and outlined in Supplemental Figure 3A-B. For lymphoid analysis, cells were first permeabilized with the FOXP3 staining kit (eBioscience, 005523) according to manufacturer's instructions.

AT2 cells were isolated and sorted as previously described (12). Briefly, perfused lungs treated with dispase (Corning # 47743-724) and DNase (50mg/mL, Sigma-Aldrich # D4513-1VL) were subjected to manual dissection. Single cell suspensions were enriched for epithelial cells using anti-EpCAM magnetic microbeads (Milteny Biotec # 130-105-958). Cells were stained with antibodies listed in Supplemental Table 4 and gated as outlined in Supplemental Figure 3C.

Native PAGE analysis

For analysis of native LUBAC formation, the Invitrogen Blue Native Gel system (Invitrogen, BN2007, BN2008) was utilized according to manufacturer's instructions and as described elsewhere (86). Briefly, cells were lysed in provided sample buffer containing 1% Digitonin and resolved on 3-12% bis-tris gel (Invitrogen, BN1001). Proteins were transferred to a PVDF membrane and immnoblotted as described above.

Cytokine determination

ELISAs were carried out on cell culture supernatants or BALF according to manufacturer's instructions using the following kits: IL-6(h) (Thermo Fisher, KHC0061C), IFN-β(h) (PBL Assay Science, 41410), IL-6(m) (Thermo Fisher, KMC0062), MCP-1(m) (Thermo Fisher EMMCP1), IFN-α(m) (PBL Assay Science, 42120), IFN-β(m) (PBL, 42400), IFN-γ(m) (Thermo Fisher, BMS606), and IL-10(m) (Thermo Fisher, EM2IL10).

Chromatin immunoprecipitation assay.

Chromatin immunoprecipitation was performed using the Simple ChIP Enzymatic Chromatin IP kit (Cell Signaling, 9003) according to manufacturer's instructions. Briefly, cells were cross-linked with formaldehyde and lysed with provided buffers. Cell lysates were subjected to sonication and nuclease treatment before immunoprecipitation with provided control IgG (5 ug) or IRF1 (10 ug, Scbt, sc-497) using provided magnetic beads. Bead eluates were then subjected to proteinase digestion and qPCR amplification of the HOIL-1L promoter (Forward: 5'TTAGCTTCAGTGTTCCCCCT-3', Reverse: 5'-CAGTGGGGAGACAATGAACAA-3') using SybrGreen (BioRad, 1708880).

Quantitative RT-PCR

Cellular mRNA was collected and purified using RNeasy mini kit (Qiagen, 74104) before cDNA preparation with qScript cDNA synthesis kit (Quanta Bio, 95047). For qRT-PCR, IQ SybrGreen master mixes (Bio-Rad, 1708880) were used according to manufacture's instructions with the primers listed in Supplemental Table 5.

Statistics

Analyses of significance were performed using GraphPad Prism (v.7.02) software. A *P* value ≤0.05 was considered statistically significant. A standard two-tailed unpaired Student's t-test was used for two groups. One-way ANOVA, followed by analysis-specific post-tests, was carried out when more than two variables were compared. Data are presented means ±s.d. overlaid with individual data points representing replicates. Statistical analysis of survival curves was performed with a two-sided log-rank (Mantel–Cox) test.

Study approval

All in vivo experiments were performed in compliance with the institutional and US National Institutes of Health guidelines and were approved by the Northwestern University Animal Care and Use Committee.

Acknowledgements

This work was supported, in part by grants sponsored by the National Heart, Lung, and Blood Institute HL071643, HL076139, and HL132454. K.I. is supported by KAKENHI from Japan Society for the Promotion of Science (Grant Number 24112002). We thank Mark Ciesielski for isolation of AT2 cells and Lynn C. Welch for her technical assistance. This work was also supported by the Northwestern University Flow Cytometry Core Facility, supported by National Cancer Institute Cancer Center Support Grant CA060553. BD FACSAria SORP

system was purchased through an NIH Grant 1S10OD011996-01. Histology services were provided by the Northwestern University Mouse Histology and Phenotyping Laboratory supported by NCI P30-CA060553 awarded to the Robert H Lurie Comprehensive Cancer Center. This work was supported by Northwestern University's Center for Advanced Microscopy and a Cancer Center Support Grant (NCI CA060553)

Contributions

P.L.B., L.A.D., and J.I.S. designed research; P.L.B., L.M.N., N.D.M., and A.V.M. performed research; K.M.R. and K.I. contributed reagents/analytic tools; P.L.B., L.A.D., J.G.N.G., A.V.M., G.R.S.B., and J.I.S., analyzed data; P.L.B., L.A.D., J.I.S., K.M.R., and G.R.S.B. discussed and edited the manuscript, and P.L.B., L.A.D., and J.I.S. wrote the manuscript.

References

1. Blank R, and Napolitano LM. Epidemiology of ARDS and ALI. *Crit Care Clin.* 2011;27(3):439.
2. Jain S, Kamimoto L, Bramley AM, Schmitz AM, Benoit SR, Louie J, Sugerman DE, Druckenmiller JK, Ritger KA, Chugh R, Jasuja S, Deutscher M, Chen S, Walker JD, Duchin JS, Lett S, Soliva S, Wells EV, Swerdlow D, Uyeki TM, Fiore AE, Olsen SJ, Fry AM, Bridges CB, Finelli L, and Pandemic Influenza AVHIT. Hospitalized patients with 2009 H1N1 influenza in the United States, April-June 2009. *N Engl J Med.* 2009;361(20):1935.
3. Napolitano LM, Park PK, Raghavendran K, and Bartlett RH. Nonventilatory strategies for patients with life-threatening 2009 H1N1 influenza and severe respiratory failure. *Crit Care Med.* 2010;38(4 Suppl):e74.
4. Rothberg MB, and Haessler SD. Complications of seasonal and pandemic influenza. *Crit Care Med.* 2010;38(4 Suppl):e91.
5. Short KR, Kroeze E, Fouchier RAM, and Kuiken T. Pathogenesis of influenza-induced acute respiratory distress syndrome. *Lancet Infect Dis.* 2014;14(1):57.
6. Vadasz I, and Sznajder JI. Gas Exchange Disturbances Regulate Alveolar Fluid Clearance during Acute Lung Injury. *Front Immunol.* 2017;8(757).
7. Herold S, Becker C, Ridge KM, and Budinger GR. Influenza virus-induced lung injury: pathogenesis and implications for treatment. *Eur Respir J.* 2015;45(5):1463.
8. Whitsett JA, and Alenghat T. Respiratory epithelial cells orchestrate pulmonary innate immunity. *Nat Immunol.* 2015;16(1):27.
9. Siren J, Imaizumi T, Sarkar D, Pietila T, Noah DL, Lin R, Hiscott J, Krug RM, Fisher PB, Julkunen I, and Matikainen S. Retinoic acid inducible gene-I and mda-5 are involved in influenza A virus-induced expression of antiviral cytokines. *Microbes Infect.* 2006;8(8):2013.
10. Kato H, Sato S, Yoneyama M, Yamamoto M, Uematsu S, Matsui K, Tsujimura T, Takeda K, Fujita T, Takeuchi O, and Akira S. Cell type-specific involvement of RIG-I in antiviral response. *Immunity.* 2005;23(1):19.
11. Davidson S, Crotta S, McCabe TM, and Wack A. Pathogenic potential of interferon alphabeta in acute influenza infection. *Nat Commun.* 2014;5(3864.
12. Peteranderl C, Morales-Nebreda L, Selvakumar B, Lecuona E, Vadasz I, Morty RE, Schmoldt C, Bespalowa J, Wolff T, Pleschka S, Mayer K, Gattenloehner S, Fink L, Lohmeyer J, Seeger W, Sznajder JI, Mutlu GM, Budinger GR, and Herold S. Macrophage-epithelial paracrine crosstalk inhibits lung edema clearance during influenza infection. *J Clin Invest.* 2016;126(4):1566.
13. Walsh KB, Teijaro JR, Wilker PR, Jatzek A, Fremgen DM, Das SC, Watanabe T, Hatta M, Shinya K, Suresh M, Kawaoka Y, Rosen H, and Oldstone MB. Suppression of cytokine storm with a sphingosine analog provides protection against pathogenic influenza virus. *Proc Natl Acad Sci U S A.* 2011;108(29):12018.
14. Lin KL, Suzuki Y, Nakano H, Ramsburg E, and Gunn MD. CCR2+ monocyte-derived dendritic cells and exudate macrophages produce influenza-induced pulmonary immune pathology and mortality. *J Immunol.* 2008;180(4):2562.
15. Arankalle VA, Lole KS, Arya RP, Tripathy AS, Ramdasi AY, Chadha MS, Sangle SA, and Kadam DB. Role of host immune response and viral load in the differential outcome of pandemic H1N1 (2009) influenza virus infection in Indian patients. *PLoS One.* 2010;5(10).
16. de Jong MD, Simmons CP, Thanh TT, Hien VM, Smith GJ, Chau TN, Hoang DM, Chau NV, Khanh TH, Dong VC, Qui PT, Cam BV, Ha do Q, Guan Y, Peiris JS, Chinh NT, Hien TT, and Farrar J. Fatal outcome of human influenza A (H5N1) is associated with high viral load and hypercytokinemia. *Nat Med.* 2006;12(10):1203.
17. Kobasa D, Jones SM, Shinya K, Kash JC, Copps J, Ebihara H, Hatta Y, Hyun Kim J, Halfmann P, Hatta M, Feldmann F, Alimonti JB, Fernando L, Li Y, Katze MG, Feldmann H, and Kawaoka Y. Aberrant innate immune response in lethal infection of macaques with the 1918 influenza virus. *Nature.* 2007;445(7125):319.
18. Oldstone MBA, Teijaro JR, Walsh KB, and Rosen H. Dissecting influenza virus pathogenesis uncovers a novel chemical approach to combat the infection. *Virology.* 2013;435(1):92.

19. Brazee PL, Soni PN, Tokhtaeva E, Magnani N, Yemelyanov A, Perlman HR, Ridge KM, Sznajder JI, Vagin O, and Dada LA. FXYD5 Is an Essential Mediator of the Inflammatory Response during Lung Injury. *Front Immunol.* 2017;8(623.
20. Tokunaga F, and Iwai K. LUBAC, a novel ubiquitin ligase for linear ubiquitination, is crucial for inflammation and immune responses. *Microbes Infect.* 2012;14(7-8):563.
21. Tokunaga F, Sakata S, Saeki Y, Satomi Y, Kirisako T, Kamei K, Nakagawa T, Kato M, Murata S, Yamaoka S, Yamamoto M, Akira S, Takao T, Tanaka K, and Iwai K. Involvement of linear polyubiquitylation of NEMO in NF-kappaB activation. *Nat Cell Biol.* 2009;11(2):123.
22. Smit JJ, Monteferrario D, Noordermeer SM, van Dijk WJ, van der Reijden BA, and Sixma TK. The E3 ligase HOIP specifies linear ubiquitin chain assembly through its RING-IBR-RING domain and the unique LDD extension. *EMBO J.* 2012;31(19):3833.
23. Brazee P, Dada LA, and Sznajder JI. Role of Linear Ubiquitination in Health and Disease. *Am J Respir Cell Mol Biol.* 2016;54(6):761.
24. Haas TL, Emmerich CH, Gerlach B, Schmukle AC, Cordier SM, Rieser E, Feltham R, Vince J, Warnken U, Wenger T, Koschny R, Komander D, Silke J, and Walczak H. Recruitment of the linear ubiquitin chain assembly complex stabilizes the TNF-R1 signaling complex and is required for TNF-mediated gene induction. *Mol Cell.* 2009;36(5):831.
25. Kirisako T, Kamei K, Murata S, Kato M, Fukumoto H, Kanie M, Sano S, Tokunaga F, Tanaka K, and Iwai K. A ubiquitin ligase complex assembles linear polyubiquitin chains. *EMBO J.* 2006;25(20):4877.
26. Ikeda F, Deribe YL, Skanland SS, Stieglitz B, Grabbe C, Franz-Wachtel M, van Wijk SJ, Goswami P, Nagy V, Terzic J, Tokunaga F, Androulidaki A, Nakagawa T, Pasparakis M, Iwai K, Sundberg JP, Schaefer L, Rittinger K, Macek B, and Dikic I. SHARPIN forms a linear ubiquitin ligase complex regulating NF-kappaB activity and apoptosis. *Nature.* 2011;471(7340):637.
27. Stieglitz B, Morris-Davies AC, Koliopoulos MG, Christodoulou E, and Rittinger K. LUBAC synthesizes linear ubiquitin chains via a thioester intermediate. *EMBO Rep.* 2012;13(9):840.
28. Rahighi S, Ikeda F, Kawasaki M, Akutsu M, Suzuki N, Kato R, Kensche T, Uejima T, Bloor S, Komander D, Randow F, Wakatsuki S, and Dikic I. Specific Recognition of Linear Ubiquitin Chains by NEMO Is Important for NF-κB Activation. *Cell.* 2009;136(6):1098.
29. Tarantino N, Tinevez JY, Crowell EF, Boisson B, Henriques R, Mhlanga M, Agou F, Israel A, and Laplantine E. TNF and IL-1 exhibit distinct ubiquitin requirements for inducing NEMO-IKK supramolecular structures. *J Cell Biol.* 2014;204(2):231.
30. Deckers J, Branco Madeira F, and Hammad H. Innate immune cells in asthma. *Trends Immunol.* 2013;34(11):540.
31. Magnani ND, Dada LA, Queisser MA, Brazee PL, Welch LC, Anekalla KR, Zhou G, Vagin O, Misharin AV, Budinger GRS, Iwai K, Ciechanover AJ, and Sznajder JI. HIF and HOIL-1L-mediated PKCzeta degradation stabilizes plasma membrane Na,K-ATPase to protect against hypoxia-induced lung injury. *Proc Natl Acad Sci U S A.* 2017;114(47):E10178.
32. Tokunaga F, Nakagawa T, Nakahara M, Saeki Y, Taniguchi M, Sakata S-i, Tanaka K, Nakano H, and Iwai K. SHARPIN is a component of the NF-[kgr]B-activating linear ubiquitin chain assembly complex. *Nature.* 2011;471(7340):633.
33. Fujita H, Tokunaga A, Shimizu S, Whiting AL, Aguilar-Alonso F, Takagi K, Walinda E, Sasaki Y, Shimokawa T, Mizushima T, Ohki I, Ariyoshi M, Tochio H, Bernal F, Shirakawa M, and Iwai K. Cooperative Domain Formation by Homologous Motifs in HOIL-1L and SHARPIN Plays A Crucial Role in LUBAC Stabilization. *Cell Rep.* 2018;23(4):1192.
34. Peltzer N, Darding M, Montinaro A, Draber P, Draberova H, Kupka S, Rieser E, Fisher A, Hutchinson C, Taraborrelli L, Hartwig T, Lafont E, Haas TL, Shimizu Y, Boiers C, Sarr A, Rickard J, Alvarez-Diaz S, Ashworth MT, Beal A, Enver T, Bertin J, Kaiser W, Strasser A, Silke J, Bouillet P, and Walczak H. LUBAC is essential for embryogenesis by preventing cell death and enabling haematopoiesis. *Nature.* 2018;557(7703):112.
35. Elton L, Carpentier I, Verhelst K, Staal J, and Beyaert R. The multifaceted role of the E3 ubiquitin ligase HOIL-1: beyond linear ubiquitination. *Immunol Rev.* 2015;266(1):208.
36. Misharin AV, Morales-Nebreda L, Mutlu GM, Budinger GR, and Perlman H. Flow cytometric analysis of macrophages and dendritic cell subsets in the mouse lung. *Am J Respir Cell Mol Biol.* 2013;49(4):503.

37. Braciale TJ, Sun J, and Kim TS. Regulating the adaptive immune response to respiratory virus infection. *Nat Rev Immunol.* 2012;12(4):295.
38. Pulendran B, and Maddur MS. Innate immune sensing and response to influenza. *Curr Top Microbiol Immunol.* 2015;386(23).
39. Queisser MA, Dada LA, Deiss-Yehiely N, Angulo M, Zhou G, Kouri FM, Knab LM, Liu J, Stegh AH, DeCamp MM, Budinger GR, Chandel NS, Ciechanover A, Iwai K, and Sznajder JI. HOIL-1L functions as the PKCzeta ubiquitin ligase to promote lung tumor growth. *Am J Respir Crit Care Med.* 2014;190(6):688.
40. Hui KP, Lee SM, Cheung CY, Mao H, Lai AK, Chan RW, Chan MC, Tu W, Guan Y, Lau YL, and Peiris JS. H5N1 influenza virus-induced mediators upregulate RIG-I in uninfected cells by paracrine effects contributing to amplified cytokine cascades. *J Infect Dis.* 2011;204(12):1866.
41. Seng LG, Daly J, Chang KC, and Kuchipudi SV. High basal expression of interferon-stimulated genes in human bronchial epithelial (BEAS-2B) cells contributes to influenza A virus resistance. *PLoS One.* 2014;9(10):e109023.
42. Portela A, and Digard P. The influenza virus nucleoprotein: a multifunctional RNA-binding protein pivotal to virus replication. *J Gen Virol.* 2002;83(Pt 4):723.
43. Tamiya H, Terao M, Takiuchi T, Nakahara M, Sasaki Y, Katayama I, Yoshikawa H, and Iwai K. IFN-gamma or IFN-alpha ameliorates chronic proliferative dermatitis by inducing expression of linear ubiquitin chain assembly complex. *J Immunol.* 2014;192(8):3793.
44. Andrilenas KK, Ramlall V, Kurland J, Leung B, Harbaugh AG, and Siggers T. DNA-binding landscape of IRF3, IRF5 and IRF7 dimers: implications for dimer-specific gene regulation. *Nucleic Acids Res.* 2018;46(5):2509.
45. Ozato K, Tailor P, and Kubota T. The interferon regulatory factor family in host defense: mechanism of action. *J Biol Chem.* 2007;282(28):20065.
46. Messeguer X, Escudero R, Farre D, Nunez O, Martinez J, and Alba MM. PROMO: detection of known transcription regulatory elements using species-tailored searches. *Bioinformatics.* 2002;18(2):333.
47. Bime C, Pouladi N, Sammani S, Batai K, Casanova N, Zhou T, Kempf CL, Sun X, Camp SM, Wang T, Kittles RA, Lussier YA, Jones TK, Reilly JP, Meyer NJ, Christie JD, Karnes JH, Gonzalez-Garay M, Christiani DC, Yates CR, Wurfel MM, Meduri GU, and Garcia JGN. Genome-Wide Association Study in African Americans with Acute Respiratory Distress Syndrome Identifies the Selectin P Ligand Gene as a Risk Factor. *Am J Respir Crit Care Med.* 2018;197(11):1421.
48. Otero JE, Dai S, Alhawagri MA, Darwech I, and Abu-Amer Y. IKKbeta activation is sufficient for RANK-independent osteoclast differentiation and osteolysis. *J Bone Miner Res.* 2010;25(6):1282.
49. Lawrence T. The Nuclear Factor NF-κB Pathway in Inflammation. *Cold Spring Harb Perspect Biol.* 2009;1(6).
50. Krammer F, and Palese P. Advances in the development of influenza virus vaccines. *Nat Rev Drug Discov.* 2015;14(3):167.
51. Lafont E, Kantari-Mimoun C, Draber P, De Miguel D, Hartwig T, Reichert M, Kupka S, Shimizu Y, Taraborrelli L, Spit M, Sprick MR, and Walczak H. The linear ubiquitin chain assembly complex regulates TRAIL-induced gene activation and cell death. *EMBO J.* 2017;36(9):1147.
52. Yarilina A, Park-Min KH, Antoniv T, Hu X, and Ivashkiv LB. TNF activates an IRF1-dependent autocrine loop leading to sustained expression of chemokines and STAT1-dependent type I interferon-response genes. *Nat Immunol.* 2008;9(4):378.
53. Ivashkiv LB, and Donlin LT. Regulation of type I interferon responses. *Nat Rev Immunol.* 2014;14(1):36.
54. Balachandran S, and Beg AA. Defining emerging roles for NF-kappaB in antivirus responses: revisiting the interferon-beta enhanceosome paradigm. *PLoS Pathog.* 2011;7(10):e1002165.
55. Szretter KJ, Gangappa S, Belser JA, Zeng H, Chen H, Matsuoka Y, Sambhara S, Swayne DE, Tumpey TM, and Katz JM. Early control of H5N1 influenza virus replication by the type I interferon response in mice. *J Virol.* 2009;83(11):5825.
56. Herold S, Steinmueller M, von Wulffen W, Cakarova L, Pinto R, Pleschka S, Mack M, Kuziel WA, Corazza N, Brunner T, Seeger W, and Lohmeyer J. Lung epithelial apoptosis in influenza virus pneumonia: the role of macrophage-expressed TNF-related apoptosis-inducing ligand. *J Exp Med.* 2008;205(13):3065.

57. Shahangian A, Chow EK, Tian X, Kang JR, Ghaffari A, Liu SY, Belperio JA, Cheng G, and Deng JC. Type I IFNs mediate development of postinfluenza bacterial pneumonia in mice. *J Clin Invest.* 2009;119(7):1910.
58. Inn KS, Gack MU, Tokunaga F, Shi M, Wong LY, Iwai K, and Jung JU. Linear ubiquitin assembly complex negatively regulates RIG-I- and TRIM25-mediated type I interferon induction. *Mol Cell.* 2011;41(3):354.
59. Belgnaoui SM, Paz S, Samuel S, Goulet M-L, Sun Q, Kikkert M, Iwai K, Dikic I, Hiscott J, and Lin R. Linear Ubiquitination of NEMO Negatively Regulates the Interferon Antiviral Response through Disruption of the MAVS-TRAF3 Complex. *Cell Host & Microbe.* 2012;12(2):211.
60. Boisson B, Laplantine E, Prando C, Giliani S, Israelsson E, Xu Z, Abhyankar A, Israel L, Trevejo-Nunez G, Bogunovic D, Cepika AM, MacDuff D, Chrabieh M, Hubeau M, Bajolle F, Debre M, Mazzolari E, Vairo D, Agou F, Virgin HW, Bossuyt X, Rambaud C, Facchetti F, Bonnet D, Quartier P, Fournet JC, Pascual V, Chaussabel D, Notarangelo LD, Puel A, Israel A, Casanova JL, and Picard C. Immunodeficiency, autoinflammation and amylopectinosis in humans with inherited HOIL-1 and LUBAC deficiency. *Nat Immunol.* 2012;13(12):1178.
61. Zinngrebe J, Rieser E, Taraborrelli L, Peltzer N, Hartwig T, Ren H, Kovacs I, Endres C, Draber P, Darding M, von Karstedt S, Lemke J, Dome B, Bergmann M, Ferguson BJ, and Walczak H. LUBAC deficiency perturbs TLR3 signaling to cause immunodeficiency and autoinflammation. *J Exp Med.* 2016;213(12):2671.
62. Zhou G, Juang SWW, and Kane KP. NK cells exacerbate the pathology of influenza virus infection in mice. *European Journal of Immunology.* 2013;43(4):929.
63. Carlin LE, Hemann EA, Zacharias ZR, Heusel JW, and Legge KL. Natural Killer Cell Recruitment to the Lung During Influenza A Virus Infection Is Dependent on CXCR3, CCR5, and Virus Exposure Dose. *Front Immunol.* 2018;9(781).
64. Duan S, and Thomas PG. Balancing Immune Protection and Immune Pathology by CD8(+) T-Cell Responses to Influenza Infection. *Front Immunol.* 2016;7(25.
65. Wells MA, Albrecht P, and Ennis FA. Recovery from a viral respiratory infection. I. Influenza pneumonia in normal and T-deficient mice. *J Immunol.* 1981;126(3):1036.
66. Arpaia N, Green JA, Moltedo B, Arvey A, Hemmers S, Yuan S, Treuting PM, and Rudensky AY. A Distinct Function of Regulatory T Cells in Tissue Protection. *Cell.* 2015;162(5):1078.
67. Mackay C, Carroll E, Ibrahim AF, Garg A, Inman GJ, Hay RT, and Alpi AF. E3 ubiquitin ligase HOIP attenuates apoptotic cell death induced by cisplatin. *Cancer Res.* 2014;74(8):2246.
68. Tang Y, Joo D, Liu G, Tu H, You J, Jin J, Zhao X, Hung MC, and Lin X. Linear ubiquitination of cFLIP induced by LUBAC contributes to TNFalpha-induced apoptosis. *J Biol Chem.* 2018;293(52):20062.
69. Fujikura D, and Miyazaki T. Programmed Cell Death in the Pathogenesis of Influenza. *Int J Mol Sci.* 2018;19(7).
70. Aguilar-Alonso F, Whiting AL, Kim YJ, and Bernal F. Biophysical and biological evaluation of optimized stapled peptide inhibitors of the linear ubiquitin chain assembly complex (LUBAC). *Bioorg Med Chem.* 2018;26(6):1179.
71. Katsuya K, Oikawa D, Iio K, Obika S, Hori Y, Urashima T, Ayukawa K, and Tokunaga F. Small-molecule inhibitors of linear ubiquitin chain assembly complex (LUBAC), HOIPINs, suppress NF-kappaB signaling. *Biochem Biophys Res Commun.* 2019;509(3):700.
72. Strickson S, Campbell DG, Emmerich CH, Knebel A, Plater L, Ritorto MS, Shpiro N, and Cohen P. The anti-inflammatory drug BAY 11-7082 suppresses the MyD88-dependent signalling network by targeting the ubiquitin system. *Biochem J.* 2013;451(3):427.
73. Yang Y, Schmitz R, Mitala J, Whiting A, Xiao W, Ceribelli M, Wright GW, Zhao H, Yang Y, Xu W, Rosenwald A, Ott G, Gascoyne RD, Connors JM, Rimsza LM, Campo E, Jaffe ES, Delabie J, Smeland EB, Braziel RM, Tubbs RR, Cook JR, Weisenburger DD, Chan WC, Wiestner A, Kruhlak MJ, Iwai K, Bernal F, and Staudt LM. Essential role of the linear ubiquitin chain assembly complex in lymphoma revealed by rare germline polymorphisms. *Cancer Discov.* 2014;4(4):480.
74. Johansson H, Isabella Tsai YC, Fantom K, Chung CW, Kumper S, Martino L, Thomas DA, Eberl HC, Muelbaier M, House D, and Rittinger K. Fragment-Based Covalent Ligand Screening Enables Rapid Discovery of Inhibitors for the RBR E3 Ubiquitin Ligase HOIP. *J Am Chem Soc.* 2019;141(6):2703.

75. Sakamoto H, Egashira S, Saito N, Kirisako T, Miller S, Sasaki Y, Matsumoto T, Shimonishi M, Komatsu T, Terai T, Ueno T, Hanaoka K, Kojima H, Okabe T, Wakatsuki S, Iwai K, and Nagano T. Gliotoxin suppresses NF-kappaB activation by selectively inhibiting linear ubiquitin chain assembly complex (LUBAC). *ACS Chem Biol.* 2015;10(3):675.
76. Muller U, Steinhoff U, Reis LF, Hemmi S, Pavlovic J, Zinkernagel RM, and Aguet M. Functional role of type I and type II interferons in antiviral defense. *Science.* 1994;264(5167):1918.
77. Boring L, Gosling J, Chensue SW, Kunkel SL, Farese RV, Jr., Broxmeyer HE, and Charo IF. Impaired monocyte migration and reduced type 1 (Th1) cytokine responses in C-C chemokine receptor 2 knockout mice. *J Clin Invest.* 1997;100(10):2552.
78. Sasaki Y, Fujita H, Nakai M, and Iwai K. Immunoblot analysis of linear polyubiquitination of NEMO. *Methods Mol Biol.* 2015;1280(297).
79. Guo X, Liu T, Shi H, Wang J, Ji P, Wang H, Hou Y, Tan RX, and Li E. Respiratory Syncytial Virus Infection Upregulates NLRC5 and Major Histocompatibility Complex Class I Expression through RIG-I Induction in Airway Epithelial Cells. 2015;89(15):7636.
80. Morales-Nebreda LI, Rogel MR, Eisenberg JL, Hamill KJ, Soberanes S, Nigdelioglu R, Cho MC, Radigan KA, Ridge KM, Misharin AV, Woychek A, Hopkinson S, Perlman H, Mutlu GM, Pardo A, Selman M, Jones JC, and Budinger GR. Lung Specific Loss of alpha3 Laminin Worsens Bleomycin-induced Pulmonary Fibrosis. *Am J Respir Cell Mol Biol.* 2014;Epub(
81. Lubarski-Gotliv I, Asher C, Dada LA, and Garty H. FXYD5 Protein Has a Pro-inflammatory Role in Epithelial Cells. *J Biol Chem.* 2016;291(21):11072.
82. Urich D, Eisenberg JL, Hamill KJ, Takawira D, Chiarella SE, Soberanes S, Gonzalez A, Koentgen F, Manghi T, Hopkinson SB, Misharin AV, Perlman H, Mutlu GM, Budinger GR, and Jones JC. Lung-specific loss of the laminin alpha3 subunit confers resistance to mechanical injury. *J Cell Sci.* 2011;124(Pt 17):2927.
83. Baer A, and Kehn-Hall K. Viral Concentration Determination Through Plaque Assays: Using Traditional and Novel Overlay Systems. *J Vis Exp.* 201493):e52065.
84. Dillon SR, Sprecher C, Hammond A, Bilsborough J, Rosenfeld-Franklin M, Presnell SR, Haugen HS, Maurer M, Harder B, Johnston J, Bort S, Mudri S, Kuijper JL, Bukowski T, Shea P, Dong DL, Dasovich M, Grant FJ, Lockwood L, Levin SD, LeCiel C, Waggie K, Day H, Topouzis S, Kramer J, Kuestner R, Chen Z, Foster D, Parrish-Novak J, and Gross JA. Interleukin 31, a cytokine produced by activated T cells, induces dermatitis in mice. *Nat Immunol.* 2004;5(7):752.
85. D'Alessio FR, Tsushima K, Aggarwal NR, West EE, Willett MH, Britos MF, Pipeling MR, Brower RG, Tuder RM, McDyer JF, and King LS. CD4+CD25+Foxp3+ Tregs resolve experimental lung injury in mice and are present in humans with acute lung injury. *J Clin Invest.* 2009;119(10):2898.
86. Wittig I, Braun HP, and Schagger H. Blue native PAGE. *Nat Protoc.* 2006;1(1):418.

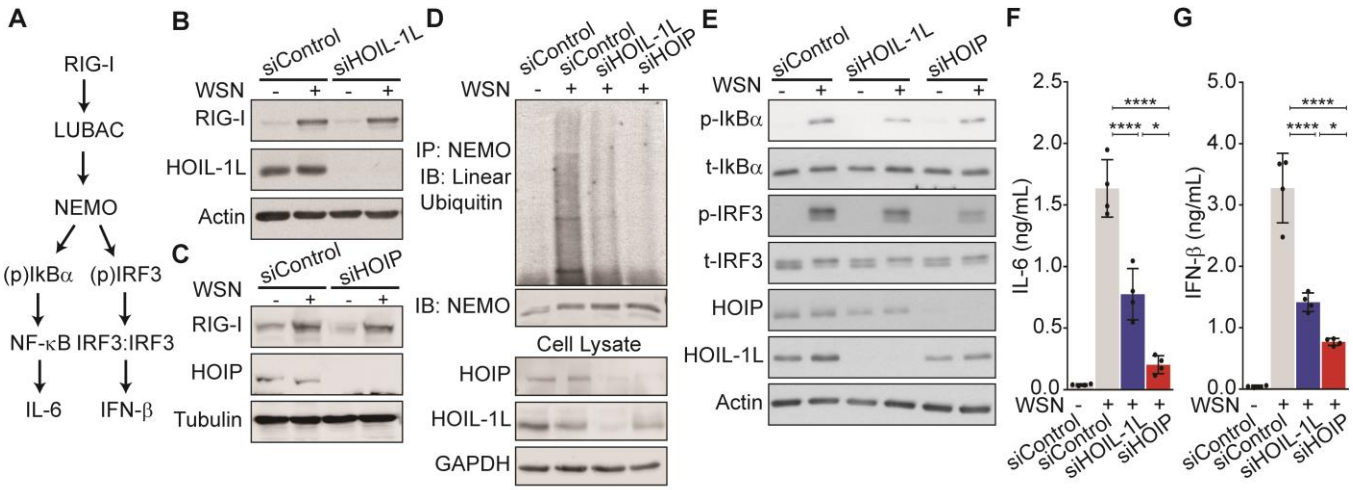

Figure 1. Linear Ubiquitin chains modulate the NF-κB response to IAV downstream of RIG-I signaling in vitro. (A) Simplified signaling pathway **(B-F)** A549 cells infected with WSN (1 MOI, 16 h) after transfection with non-targeting siRNA (siControl) or siRNA against either HOIL-1L or HOIP. **(B-E)** Representative immunoblots of **(B-C)** RIG-I activation (n=4). **(D)** Linear ubiquitination of NEMO (n=3) **(E)** p-IkBα, total IkBα, p-IRF3, total IRF3 (n=4). **(F-G)** Cytokines in the supernatant were determined by ELISA **(F)** IL-6 (n=4) **(G)** IFN-β (n=4). Mean ± s.d. overlaid with individual data points representing replicates are depicted, **P* < 0.05, ***P* < 0.01, ****P* < 0.005, *****P* < 0.0001 (one-way ANOVA, Bonferroni post-hoc test).

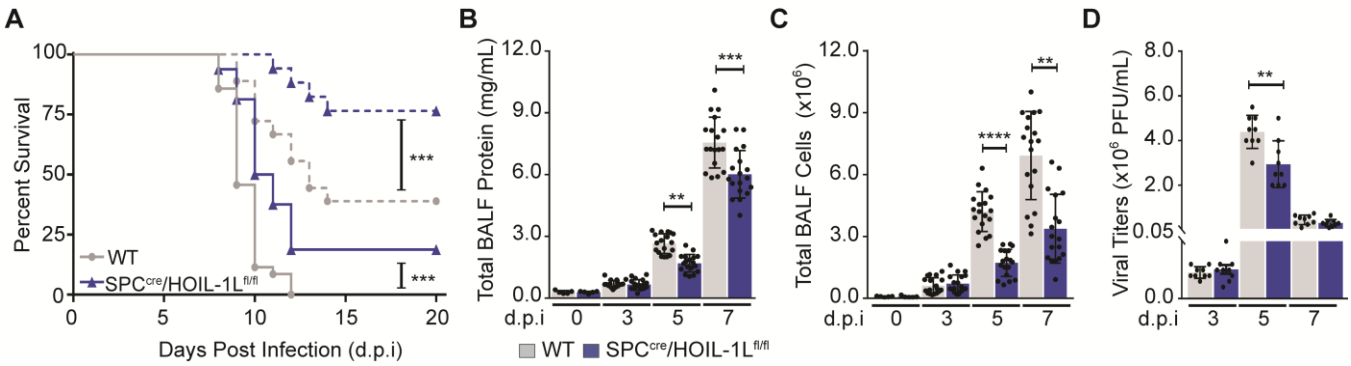

Figure 2. Loss of HOIL-1L from the alveolar epithelium improves survival and reduces lung injury in mice infected with IAV. (A) Survival of WT and SPC^{cre}/HOIL-1L$^{fl/fl}$ mice infected with a low (n=18, dashed line) or lethal (n=30, solid line) dose of WSN. **(B-C)** BALF was collected at 0 (n=5), 3, 5 and 7 d.p.i. (n=18) with a lethal dose of WSN and analyzed for **(B)** total protein concentration and **(C)** cellular infiltration. (**D**) Quantification of viral titers in WT and SPC^{cre}/HOIL-1L$^{fl/fl}$ mice at 3, 5, and 7 d.p.i. (n=9). Mean ± s.d. overlaid with individual data points representing replicates are depicted, **P* < 0.05, ***P* < 0.01, ****P* < 0.005, *****P* < 0.0001 (**A**, two-tailed log-rank Mantel-Cox test; **B-D**, one-way ANOVA, Bonferroni post-hoc test).

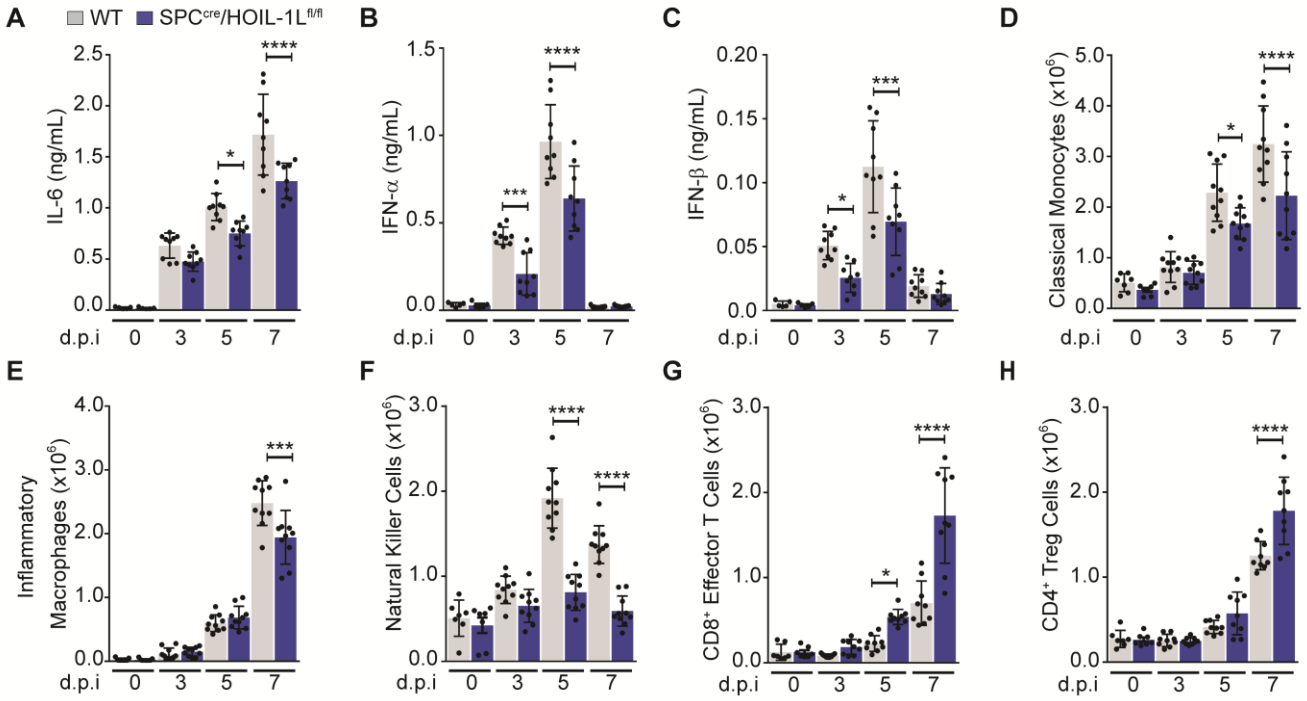

Figure 3. Alveolar epithelial loss of HOIL-1L reduces the inflammatory response in IAV infected mice. WT and SPC^{cre}/HOIL-1L$^{fl/fl}$ mice were infected with a lethal dose of WSN. **(A-C)**. BALF at 0 (n=5), 3, 5 and 7 d.p.i. (n=9) was analyzed by ELISA for **(A)** IL-6 **(B)** IFN-α **(C)** IFN-β **(D-H)** Lung immune cell populations at 0 (n=7), 3, 5 and 7 (n=10) d.p.i. analyzed by flow cytometry for **(D)** CD11b^{hi}MHCII^{low}Ly6C^{hi} classical monocytes **(E)** CD11b^{hi}MHCII^{hi}CD24^{low}CD64^{hi} inflammatory macrophages **(F)** NK1.1^{+}CD11b^{hi}CD24^{hi} natural killer cells **(G)** CD44^{+}CD62L^{-}CD8^{+} T cells **(H)** CD4^{+}CD25^{+}Foxp3^{+} T_{reg} cells. Mean ± s.d. overlaid with individual data points representing replicates are depicted, *P < 0.05, **P < 0.01, ***P < 0.005, ****P < 0.0001 (one-way ANOVA, Bonferroni post-hoc test).

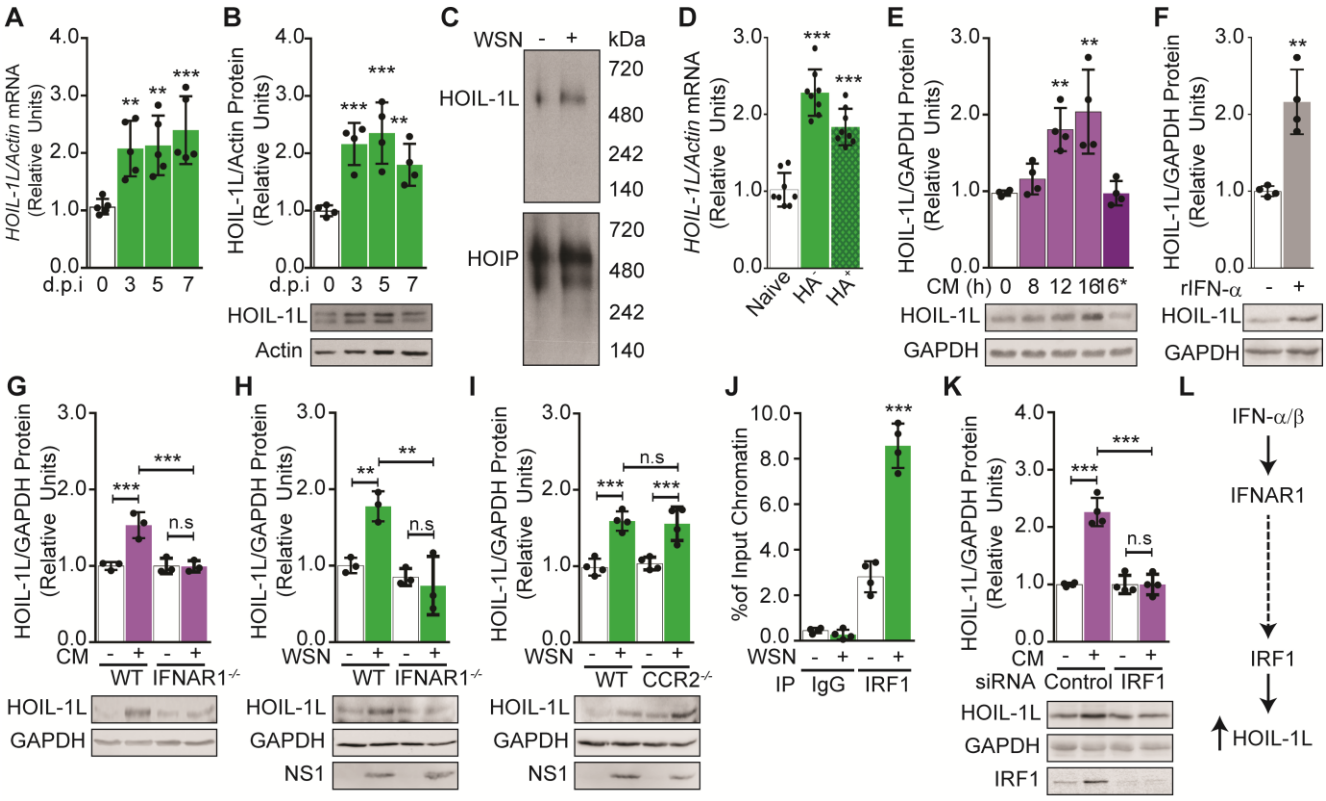

Figure 4. HOIL-1L is upregulated during IAV infection though a type I interferon receptor signaling axis. (A-B) AT2 cells isolated from WT mice 0, 3, 5 and 7 d.p.i. **(A)** HOIL-1L mRNA (n=5) **(B)** Representative HOIL-1L immunoblot and its quantification (n=4). **(C)** Representative native PAGE immunoblot of HOIL-1L and HOIP expression in AT2 cells infected in vitro with WSN (n=3). **(D)** HOIL-1L mRNA expression in AT2 cells from WT mice 0 and 3 d.p.i. sorted based on expression of the viral protein HA (n=8). **(E-I)** Representative HOIL-1L immunoblot and quantification in **(E)** A549 cells treated for 0, 8, 12 and 16 hours with conditioned media (CM), * indicated boiled CM (n=4). **(F)** A549 cells treated with recombinant IFN-α (n=4). **(G)** AT2 cells isolated from WT and IFNAR1$^{-/-}$ mice treated in vitro with CM (n=3) **(H-I)** AT2 isolated from WT and **(H)** IFNAR1$^{-/-}$ mice treated in vitro with WSN (n=3) **(I)** CCR2$^{-/-}$ mice treated in vitro with WSN (n=4) **(J)** qRT-PCR quantification of HOIL-1L promoter after ChIP of IRF1 in A549 cells (n=4) **(K)** Representative HOIL-1L immunoblot and quantification in siControl or siIRF1 transfected A549 cells treated with CM (n=4) **(L)** Proposed type I IFN pathway leading to HOIL-1L upregulation. Mean ± s.d. overlaid with individual data points representing replicates depicted, *P < 0.05, **P < 0.01, ***P < 0.005, ****P < 0.0001 (one-way ANOVA, Bonferroni post-hoc test).

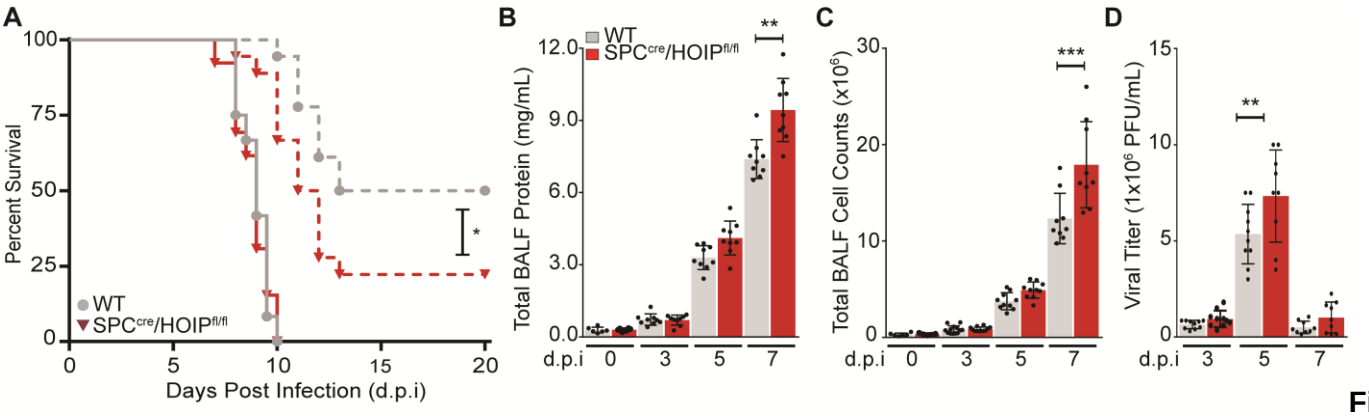

Figure 5. Loss of HOIP from the alveolar epithelium decreases survival and enhances lung injury in mice infected with IAV. (A) Survival of WT and SPC^{cre}/HOIP$^{fl/fl}$ mice infected with a low (n=18, dashed line) or lethal (n=13, solid line) dose of WSN. **(B-C)** BALF was collected from at 0, 3, 5 and 7 d.p.i. (n=9) and analyzed for **(B)** total protein concentrations and **(C)** cellular infiltration. **(D)** Quantification of viral titers in WT and SPC^{cre}/HOIP$^{fl/fl}$ at 3, 5, and 7 d.p.i. (n=9). Mean ± s.d. overlaid with individual data points representing replicates are depicted *P < 0.05, **P < 0.01, ***P < 0.005, ****P < 0.0001 (**A**, two-tailed log-rank Mantel-Cox test; **B-D**, one-way ANOVA, Bonferroni post-hoc test).

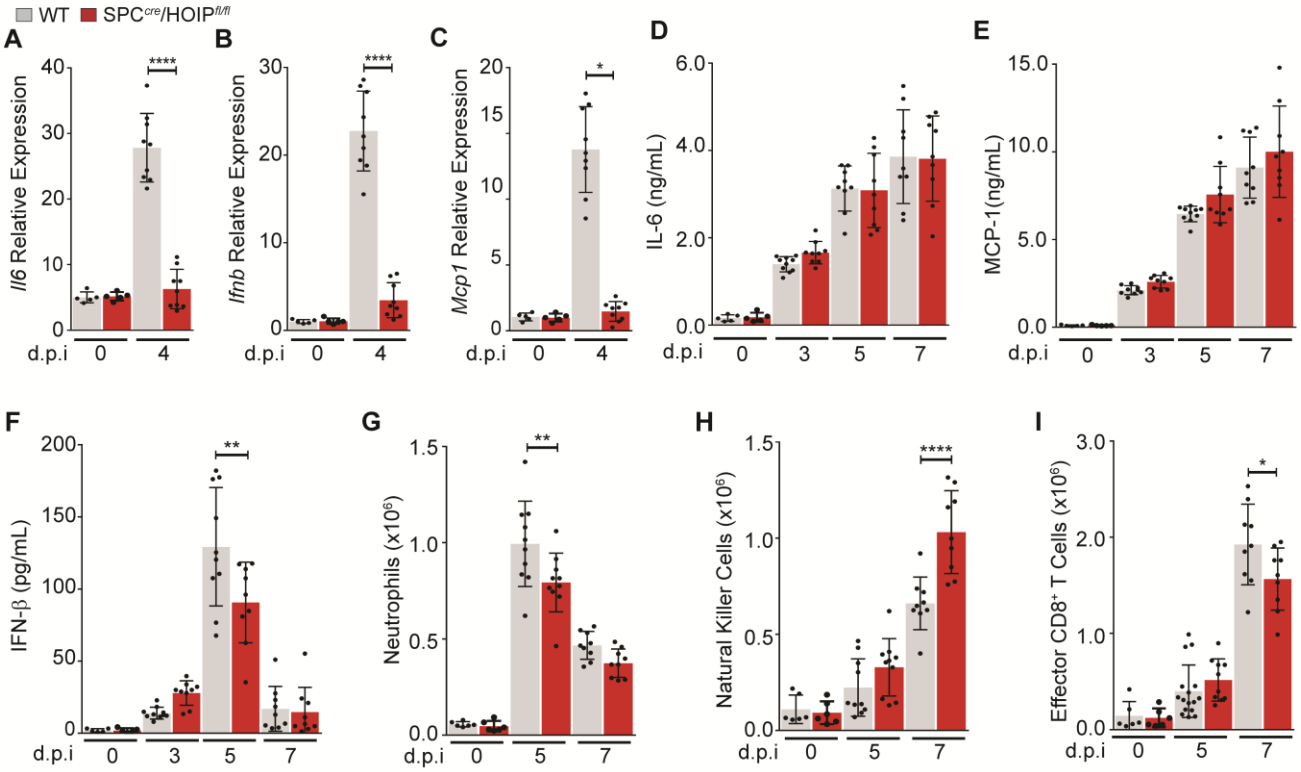

Figure 6. **Loss of HOIP from the alveolar epithelium inhibits alveolar epithelial driven inflammatory response to IAV infection**. **(A-G)** WT and SPC^{cre}/HOIP$^{fl/fl}$ mice infected with a lethal dose of WSN **(A-B)** AT2 cells at 0 and 4 d.p.i. (n=9) analyzed for **(A)** *Il6* mRNA **(B)** *Mcp1* mRNA **(C)** *Ifnb* mRNA. **(D-F)** BALF analyzed by ELISA at 0, 3, 5, 7 d.p.i. (n=9) for **(D)** IL-6 **(E)** MCP-1 **(F)** IFN-β. **(G-I)** Lung immune cell populations at 0, 5 and 7 (n=9) d.p.i. analyzed by flow cytometry for **(G)** Ly6G^{+}CD11b^{+}CD24^{+} Neutrophils **(H)** NK1.1^{+}CD11b^{hi}CD24^{hi} natural killer cells **(I)** CD44^{+}CD62L^{-}CD8^{+} T cells. Mean ± s.d overlaid with Individual data points representing replicates are depicted, **P* < 0.05, ***P* < 0.01, ****P* < 0.005, *****P* < 0.0001. (one-way ANOVA, Bonferroni post-hoc test)

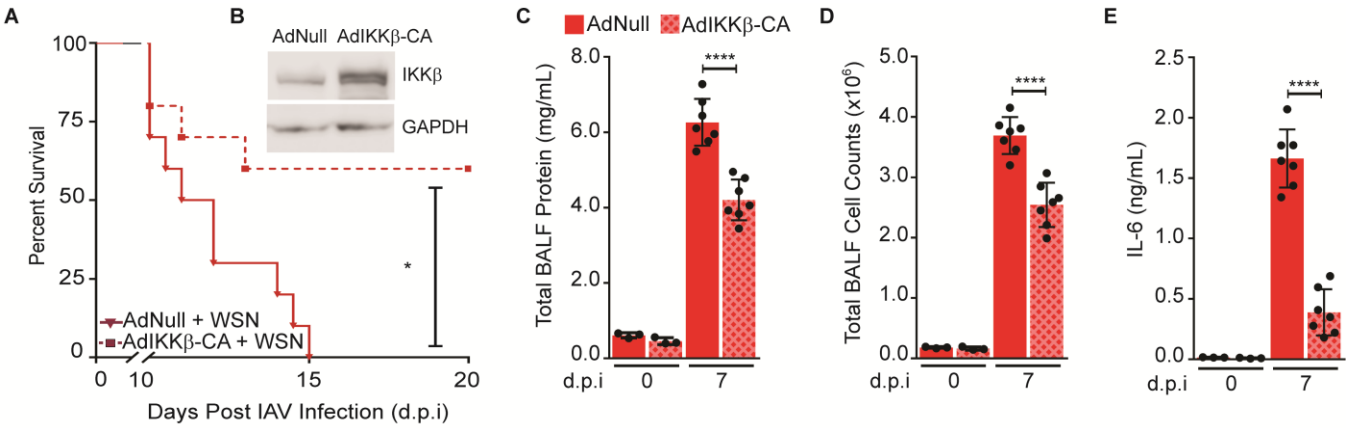

Figure 7. Restoration of NF-κB pathway in SPC^{cre}/HOIP$^{fl/fl}$ mice improves survival in response to IAV infection (A) Survival curve of SPC^{cre}/HOIP$^{fl/fl}$ mice administered either AdNull (n=11, solid line) or AdIKK-β-CA (n=10, dashed line) followed by low dose WSN. **(B)** Immunoblot of AT2 cell lysates showing overexpression of IKKβ (n=3) **(C-E)** BALF from SPC^{cre}/HOIP$^{fl/fl}$ mice administered either AdNull or AdIKK-β-CA collected at 0 (n=3), and 7 d.p.i. (n=7) of low dose of WSN and analyzed for **(C)** total protein concentration, **(D)** cellular infiltration and (**E**) IL-6. Mean ± s.d overlaid with Individual data points representing replicates are depicted, **P* < 0.05, ***P* < 0.01, ****P* < 0.005, *****P* < 0.0001. (**A**, two-tailed log-rank Mantel-Cox test; **C-E**, one-way ANOVA, Bonferroni post-hoc test).

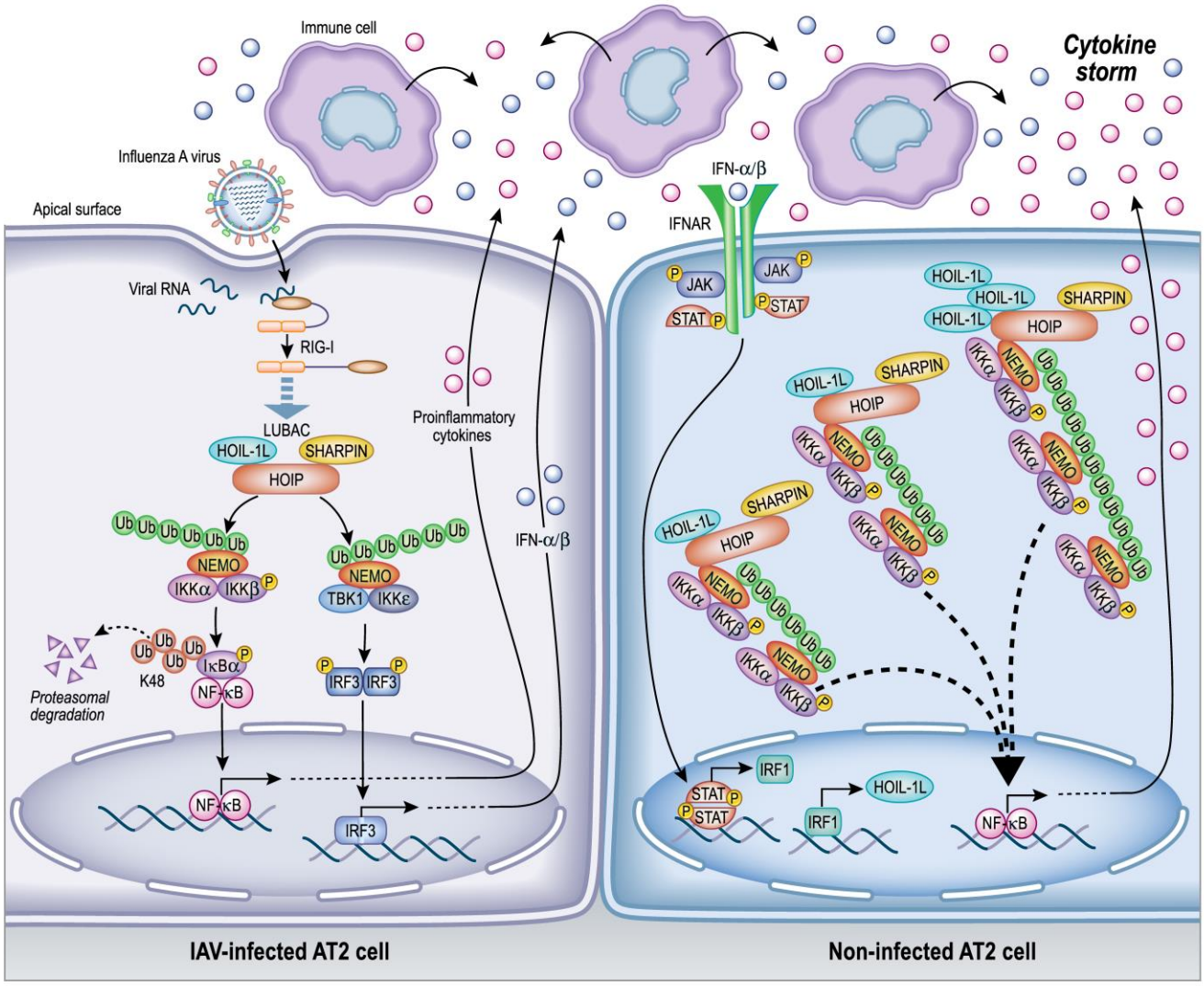

Figure 8. Cartoon representing HOIL-1L upregulation via IRF1 in AT2 cells Upon IAV infection, LUBAC-dependent activation of NF-κB and IRF3 pathways occurs downstream of RIG-I. Subsequent release of pro-inflammatory cytokines and type 1 interferons recruit immune cells to the airspace, contributing to the growing cytokine storm. In non-infected AT2 cells, IFN secreted either by epithelial cells or the recruited immune cells, binds to IFNAR1 triggering a signal cascade that upregulates HOIL-1L via IRF1. Newly synthesized HOIL-1L may either contribute to increased number of LUBAC complexes or a change in LUBAC stoichiometry to include a higher ratio of HOIL-1L within the complex. Both situations result in LUBAC increased stability and exaggerated production of cytokines which contributes to the morbidity and mortality observed in severe cases of influenza infection.